A TRANSFERABLE BIO-OPTICAL MODEL FOR QUANTIFICATION OF INLAND WATER CAYNOBACTERIAL PIGMENTS

Linhai Li

Submitted to the faculty of the University Graduate School
in partial fulfillment of the requirements
for the degree
Master of Science
in the Department of Earth Sciences,
Indiana University

August 2011

Accepted by the Faculty of Indiana University, in partial fulfillment of the requirements for the degree of Master of Science.

Lin Li, Ph.D., Chair

Master's Thesis Committee

Lenore P. Tedesco, Ph.D.

Jeffrey S. Wilson, Ph.D.

ACKNOWLEDGEMENTS

First and foremost, I would like to thank my parents. They have worked so hard to provide me as many resources as they can to support my life and education. Without their sacrifices, I could not continue my education in China and be accepted by Wuhan University two years ago, not mention to accomplish my master degree in IUPUI. I dedicate this thesis to my great parents.

I appreciate the assistance and hard work of my graduate committee, especially my advisor and graduate chair, Dr. Lin Li. I have learned much from all three members.

I am also thankful to Bob Hall, Nicolas Clercin, Angie Cowan, Mike Stouder, Jake Lemon and other staff for assisting field campaigns and *in situ* data collection.

I thank all the workmates in Lab SL037, Kaishan Song, Tingting Zhang, Shuai Li, Zuchuan Li, Dawei Liu, Ying Sun, for helping analyze samples in laboratory.

I am truly grateful to the faculty, staff and other students of Department of Earth Science for easing my life and study at IUPUI.

At last, I also thank the financial support from NASA Energy and Water Cycle Study program (Grant No. NNX09AU87G) and all others who I missed above but gave me help.

ABSTRACT

Linhai Li

A TRANSFERABLE BIO-OPTICAL MODEL FOR QUANTIFICATION OF INLAND WATER CAYNOBACTERIAL PIGMENT

Cyanobacterial blooms are currently one of the most important issues faced by environmental agencies, water authorities and public health organizations. Remote sensing provides an advanced approach to monitor cyanobacteria by detecting and quantifying chlorophyll-a (Chl-*a*) and phycocaynin (PC). In this thesis, an analytical bio-optical model, more typically applied to ocean waters, was modified to accommodate the complexity of inland waters. The newly developed models work well to estimate inherent optical properties, including absorption and backscattering coefficients, in eight different study sites distributed around the globe. Based on derived absorption coefficients, Chl-*a* and PC concentrations were accurately retrieved for data sets collected annually from 2006 to 2010, and the estimation accuracy exceeded that of currently used algorithms. An important advantage of the model is that low concentrations of Chl-*a* and PC can be predicted more accurately, enabling early warning of cyanobacterial blooms. In addition, the results also indicated good spatial and temporal transferability of the algorithms, since no specific calibration procedures were required for data sets collected in a different sites and seasons. The compatibility of the newly developed algorithm with MERIS spectra provides the possibility for routine surveillance of cyanobacterial growth in inland waters.

Lin Li, Ph.D, Chair

TABLE OF CONTENTS

LIST OF TABLES viii

LIST OF FIGURES ix

I. GENERAL INTRODUCTION 1

II. A GLOBALLY TRANSFERABLE MODEL FOR INLAND WATERS (I): DERIVING INHERENT OPTICAL PROPERTIES AND QUANTIFYING CHLOROPHYLL-A 6

ABSTRACT 6

1. Introduction 7

1.1 Deriving the inherent optical properties (IOPs) 7

1.2 Estimation of chlorophyll-a concentration 11

1.3 Objectives of this study 12

2. Data collection 12

2.1 Study sites 12

2.2 Remote sensing reflectance measurements 14

2.3 Chl-a and total suspended matter concentration measurements 18

2.4 Absorption coefficients measurements 19

3. Model for IOPs inversion 20

4. Model for Chl-*a* retrieval 23

5. Results and discussion 25

5.1 Derived Absorption Coefficient 25

5.2 Backscattering 29

5.3 Chlorophylls 31

5.3.1 Chlorophylls estimation 31

5.3.2 Factors interfering with Chl-a retrieval 37

5.4 Application on simulated MERIS spectra 39

6. Conclusions 40

Acknowledgements 41

III. A GLOBALLY TRANSFERABLE MODEL FOR INLAND WATERS (II): PARTITIONING NON-WATER ABSORPTION COEFFICIENTS AND ESTIMATING PHYCOCYANIN 42

ABSTRACT 42

1. Introduction 43

2. Materials and Methods 46

2.1. Study sites 46

2.2. Reflectance measurement 47

2.3. Pigments extraction and quantification 48

2.4. Absorption coefficient in laboratory 49

2.5. Remotely deriving absorption coefficients of phytoplankton, CDM and PC 52

2.6 Retrieval of phycocyanin concentration 57

3. Results 59

3.1. Retrieval of $a_{ph}(\lambda)$ and $a_{cdm}(\lambda)$ 59

3.2. Estimation of PC concentration 61

4. Discussion 62

4.1. Absorption partitioning methods for inland waters 62

4.2. Factors influencing the estimation of PC 65

4.3. Application on simulated MERIS reflectance 67

5. Conlusions 68

Acknowledgements 69

IV. CONCLUSIONS 70

REFERENCES 72

CURRICULUM VITAE

LIST OF TABLES

Table 2.1. Symbols and abbreviations. ····· 9

Table 2.2. The sampling date, number of samples and ranges of measured Chl-*a* and TSM as well as absorption and backscattering parameters. ····· 16

Table 2.3. Globally transferable model (GTM) for deriving the inherent optical properties (IOPs) and Chl-*a* concentration. ····· 24

Table 2.4. Evaluation of Chl-*a* estimation from GTM-estimated $a_{t\text{-}w}(\lambda)$ using equation 18 and equation 19. LT=Lake Tai, SR=Shitoukoumen Reservoir, Aus= Sites in Australia, IN08=Sites in Indiana 2008, IN10=Sites in Indiana 2010. ····· 32

Table 2.5. GTM-Estimated $a^*_{ph}(665)$ for the investigated sites and that by Gons et al. (2008). $a^*_{ph}(665)$ are estimated by dividing estimated $a_{t\text{-}w}(665)$ with measured Chl-*a*. ····· 35

Table 3.1. List of symbols and acronyms. ····· 46

Table 3.2. Statistical information of pigments concentrations and PC:Chl-*a* ratio. ····· 47

Table 3.3. Globally transferable model (GTM) to derive IOPs and Chl-*a* concentration. ····· 56

Table 3.4. Extended steps of GTM to estimate $a_{cdm}(\lambda)$, $a_{ph}(\lambda)$ and PC. ····· 57

Table 3.5. The comparison of the partitioning methods. C06=Ciotti & Bricaud et al. (2006), O07=Oubelkheir et al (2007) and W09=Wang et al. (2009). ····· 64

LIST OF FIGURES

Fig. 2.1. Above ($R_{rs}(\lambda)$) and below ($r_{rs}(\lambda)$) surface remote sensing reflectance spectra measured instudy sites. ····· 17

Fig. 2.2. A: measured $a_{t\text{-}w}(\lambda)$; B: measured $a_{cdom}(\lambda)$. Both $a_{t\text{-}w}(\lambda)$ and $a_{cdom}(\lambda)$ are only available for samples collected in Indiana sites 2010, and 40 samples were dumped because of inappropriate storage. ····· 20

Fig. 2.3. Measured $a_{sol}(\lambda)$ of samples collected in Indiana 2010. $a_{sol}(\lambda)$ is also referred as *in vitro* $a_{ph}(\lambda)$. ····· 20

Fig. 2.4. A: GTM-estimated $a_{t\text{-}w}(\lambda)$ vs. wavelength for samples with highest and lowest Chl-*a* at each site. IN08 = Indiana 2008; IN10 = Indiana 2010; Aus = Australia. MIN means minimal Chl-*a* and MAX means maximal Chl-*a*; B, C and D: GTM-estimated $a_{t\text{-}w}(\lambda)$ vs. measured $a_{t\text{-}w}(\lambda)$ for featured bands. ····· 27

Fig. 2.5. A: Comparison between estimated $a_{t\text{-}w}(\lambda)$ using QAA and measured $a_{t\text{-}w}(\lambda)$ for smaples collected in Indiana sites 2010; B, C, D: QAA-estimated $a_{t\text{-}w}(\lambda)$ vs. wavelength for featured bands. ····· 29

Fig. 2.6. GTM-estimated backscattering coefficients. A: the maximal (MAX) and minimal (MIN) $b_{bp}(\lambda)$ for the sites including Indiana (IN08 & IN10), Lake Tai (LT) and Shitokoumen (SR) in China, and Australia (AU); B: variability of estimated Y for each site. ····· 30

Fig. 2.7. Comparison between measured Chl-*a* and estimated Chl-*a* by equation 18. ···· 33

Fig. 2.8. Estimated *in vivo* $a_{ph}(665)$ (=$a_{t\text{-}w}(665)$) vs. measured *in vitro* $a_{ph}(665)$ (also $a_{sol}(665)$). *In vitro* peak at 665 nm is corresponding to *in vivo* peak 675 nm due to the band shift effect. This figure shows the conversion between *in vivo* $a_{ph}(665)$ and *in vitro* $a_{ph}(665)$. ····· 35

Fig. 2.9. Comparison between relative error (RE, equation 21) and possible interfering factor for estimating Chl-*a*. Each figure shows the RE resulted from estimation by equation 18 and equation 19, respectively. A: RE vs. $a_{cdom}(440)$; B: RE vs. NAP; C: Relative error vs. Chl-*a*/TSM. ····· 36

Fig. 2.10. A: Simulated MERIS imagery spectra; B: GTM-estimated $a_{t\text{-}w}(\lambda)$ based on A; C: estimated Chl-*a* vs. measured Chl-*a* using equation 24; D: estimated Chl-*a* vs. measured Chl-*a* using equation 19. ····· 40

Fig. 3.1. Measured below surface remote sensing reflectance $r_{rs}(\lambda)$. PE: depression due to phycoerythrin (PE) absorption; PC: depression due to PC absorption. ····· 48

Fig. 3.2. A: *in vivo* $a_{ph\text{-}pc}(\lambda)$ by adjusting $a_{sol}(\lambda)$ measured in 90% acetone extraction; B: regression coefficients (left axis) and R^2 (right axis) for equation 4 using dataset in A. ····· 50

Fig. 3.3. A: measured $a_{t\text{-}w}(\lambda)$ from unfiltered water samples; B: measured $a_{cdm}(\lambda)$; C: measured $a_{ph}(\lambda)$. Forty samples are excluded due to inappropriate storage and total 151 samples are shown in this figure. ····· 52

Fig. 3.4. Estimated $a_{t\text{-}w}(\lambda)$ using GTM for all samples collected in Indiana 2010. ····· 56

Fig. 3.5. A: retrieved $a_{cdm+pc}(\lambda)$ which includes absorption of CDM, PC, PE. PE is not soluble in acetone either. B: modeled $a_{cdm}(\lambda)$ from A. The absorption peaks of pigments, those not soluble in acetone are eliminated. C: modeled $a_{ph\text{-}pc}(\lambda)$ using equation 4 with GTM-estimated $a_{ph\text{-}pc}(675)$. D: estimated $a_{ph}(\lambda)$ which contains absorption features of all pigments. ····· 60

Fig. 3.6. Comparison between measured and estimated absorption coefficients for featured bands. A: estimated $a_{cdm}(443)$ vs. measured $a_{cdm}(443)$; B: estimated $a_{ph}(443)$ vs. measured $a_{ph}(443)$; C: estimated $a_{ph}(620)$ vs. measured $a_{ph}(620)$; D: estimated $a_{ph}(675)$ vs. measured $a_{ph}(675)$. Dash line represents 1:1 line. ····· 61

Fig. 3.7. Comparison between measured and estimated PC concentrations. A: by approach in this study; B:by semi-empirical algorithm developed by Simis et al. (2005). Dash line represents 1:1 line, and solid line is regression line. ····· 62

Fig. 3.8. Evaluation of the accuracy of GTM-estimated Chl-*a* vs. measured Chl-*a*. Dash line represents 1:1 line, and solid line is regression line. ····· 64

Fig. 3.9. The relationship between relative error (RE; equation 15) and PC:Chl-*a*. A: RE for the estimation by approach in this study; B: RE for the estimation by semi-empirical algorithm developed by Simis et al. (2005). ····· 67

Fig. 3.10. Results based on simulation of MERIS reflectance from hyperspectral measurements. A: simulated MERIS remote sensing reflectance; B: estimated $a_{cdm}(\lambda)$; C: estimated $a_{ph}(\lambda)$; D: estimated PC vs. measured PC. ····· 68

I. GENERAL INTRODUCTION

Cyanobatecria, the largest and most diverse group of prokaryotes, can multiply very quickly in the warm summer, when temperature, light and nutrient runoff from agriculture fertilizer or other nutrient sources increase (Mishra et al., 2009). Because of their colored pigments, chlorophylls (green) and phycocyanin (blue), cyanobacteria are known as blue-green algae. Cyanobacteria usually dominate the phytoplankton in lakes, estuaries, and reservoirs, due to several key adaptations that include buoyancy regulation, elementary nitrogen fixing capability, and efficient use of yellow-orange light for photosynthesis (Jupp et al., 1994; Paerl & Huisman, 2009; Reynolds & Walsby, 1975), which make cyanobateria be main species present in eutrophic inland waters. In the eutrophic waters dominated by cyanobacteria, recreational activities and aquatic habitats are frequently impacted due to the development of thick surface scums, the development of taste and odor compounds, such as geosmin and 2-methylisoborneol, and human and animals' health may be threatened by the cyanotoxins (Codd et al., 1999; Kuster et al., 2006; Mishra et al., 2009; Randolph et al., 2008). Therefore, cyanobacterial blooms are one of the most important issues faced by environmental agencies, water authorities and public health organizations (Backer, 2002).

Traditional methods for monitoring water quality consist of field sample collection, laboratory analysis, and identification of phytoplankton, and thus are time consuming, labor intensive and expensive. Collecting water samples that are representative of the phytoplankton community in the water column is not easy to achieve because some cyanobacteria regulate their buoyancy to form either dense accumulations just below the water surface or surface scum (Sellner, 1997) and a floating ship could disturb the natural

spatial distribution of a bloom (Kutser, 2004) unless a special sampling method is used (Metsamaa et al., 2006). In addition, predicting the location and timing of algal blooms using traditional field sampling methods is extremely difficult because algal blooms may be ephemeral, persisting for only a few days.

Remote sensing provides an alternative means of monitoring cyanobateria blooms in ocean water and inland waters with space-borne satellite imagery, air-borne imagery and field spectrometric data. Metsamaa et al. (2006) stated that remote sensing is potentially the only way to map the spatial distribution and estimate the amount of cyanobacteria during bloom conditions when the biomass is concentrated just below the water surface, though remote sensing sensors can't penetrate the extremely thick accumulation layer of cyanobacterial (Kutser, 2004). Moreover, remote sensing can be used to generate water quality maps of cyanobateria blooms that enable drinking water managers to quickly assess water quality and allow for improved management decisions.

The first task of monitoring cyanobacterial blooms with remote sensing is to detect and quantify chlorophyll-a (Chl-*a*) and phycocyanin (PC) based on their optical properties. Chl-*a*, a photosynthetic pigment present in all autotrophic species is a general indicator for phytoplankton biomass. Chl-*a* has an absorption maximum at around 440 nm and 670 nm, from which Chl-*a* concentrations could be estimated (e.g. Dekker, 1993; Gitelson et al., 2007; Gons, 1999; Simis et al., 2005). PC is the accessory pigment that provides a reliable signature of cyanobacteria in inland waters. PC plays a significant role in cyanobacterial light adaptation, which gives cyanobacteria a competitive advantages so that they can dominate algal species (Jupp et al., 1994). PC has an absorption peak

around 620 nm, from which PC concentration in cyanobacteria could be estimated (Dekker et al., 1993; Randolph et al., 2008; Simis et al., 2005; Schalles & Yacobi, 2000).

Morel and Gordon (1980) summarized three types of approaches to retrieving water quality parameters, including Chl-*a* and PC concentrations, from remote sensing data. The first two are empirical and semi-empirical approaches that are based on statistical relationships between apparent optical properties (AOPs), e.g. the works listed above for Chl-*a* and PC retrieval. Both empirical and semi-empirical models describe relationships of single bands, band combinations or band ratios to water quality parameters. These types of models require water quality data with concurrent remote sensing data for calibration, and use linear, exponential or polynomial relationships. In spite of resulting in high coefficients of determination (R^2), these models are site- and data- specific and have difficulties being transferred spatially and temporally. The bio-optical model, a third approach, is believed to have better spatial, temporal and instrumental transferability than empirical and semi-empirical methods because a bio-optical model is often based on the relationship of inherent optical properties (IOPs) and AOPs.

The transferability of the bio-optical model depends on the variability of IOPs because IOPs have significant influences on the reflectance spectra (Mishra et al., 2009; Mao et al., 2010). Both the specific absorption and backscattering coefficients of individual water quality constituents could vary with a change of their physical state and environmental conditions. To be more specific, for phytoplankton specific absorption coefficients, $a^*_{ph}(\lambda)$, different cell sizes result in different package effects (Babin et al., 2003; Sathyendranath et al., 1987), which could explain the magnitude difference of $a^*_{ph}(\lambda)$ among various phytoplankton species. Similar observations have been made by

Babin and Stramski (2004), Ruiz-Verdu et al. (2008a) and Mao et al. (2010). Differences in the pigments contained in different species could explain variations of spectra shape of $a^*_{ph}(\lambda)$ (Ruiz-Verdu et al., 2008a; Subramaniam et al., 1999b; Zhang et al., 2010). Even from oligotrophic water to eutrophic water, $a^*_{ph}(\lambda)$ also varies because of different Chl-*a* concentrations (Babin et al., 2003). Meanwhile, the absorption of tripton (TR), $a_{tr}(\lambda)$, and colored dissolved organic matter (CDOM), $a_{cdom}(\lambda)$, could be expressed as an exponential function with 440 nm as a reference wavelength, i.e., $a_x(\lambda)=a_x(440)\exp[-S_x\times(\lambda-440)]$ (x stands for TR or CDOM, S_x is the slope). The slope S_x reflects the variations of $a_{tr}(\lambda)$ and $a_{cdom}(\lambda)$. In fact, $a_{tr}(\lambda)$ shows variations among different types and sizes (Babin & Stramski, 2004; Bricaud et al., 1998; Prieur & Sathyendranath, 1981). Babin et al. (2003) also suggested that the relative proportion of organic and inorganic matter in TR might be the reason causing the variations of S_{tr}. S_{CDOM} exhibits variations in response to different salinity concentration (Gallegos et al., 2005; Keith et al., 2002), and phytoplankton species from which CDOM is derived (Keith et al., 2002). In addition, S_{CDOM} for fulvic acid is about two times that of humic acid (Carder et al., 1989).

IOPs of water constituents vary both spatially and temporally, because phytoplankton, TR and CDOM compositions are not expected to be similar across different lakes, reservoirs or estuaries during different seasons. It is the IOPs variations that result in the optical complexity of inland waters. The objectives of this thesis include:

1) Modifying an analytical bio-optical model to accommodate the complexity of inland waters and improving the IOPs estimation accuracy;

2) Developing a new partitioning approach to separate PC and Chl-*a* related absorption coefficients;

3) Investigating the feasibility of applying laboratory based quantification methods on bio-optical model derived pigments' absorption coefficients;

4) Studying the performance of a bio-optical model on detecting cyanobacterial blooms in different sites and seasons.

II. A GLOBALLY TRANSFERABLE MODEL FOR INLAND WATERS (I): DERIVING INHERENT OPTICAL PROPERTIES AND QUANTIFYING CHLOROPHYLL-A [*]

ABSTRACT

In-water inherent optical properties (IOPs) are the most significant factors affecting the light propagation within water column. Obtaining IOPs, including absorption and backscattering coefficients, facilitates the estimation of aquatic biomass, primary production, heat flux, and carbon pools. In addition, chlorophyll-a (Chl-*a*) concentration is also recommended to be determined from IOPs in inland waters, because empirical and some semi-empirical algorithms that directly start from remote sensing reflectance are usually limited to sites where they were derived. Therefore, establishing models that predict IOPs and Chl-*a* from retrieved IOPs is of significance for understanding the bio-optical properties and occurrence of algal blooms in eutrophic reservoirs, lakes and estuaries makes, respectively. In this paper, a globally transferable model (GTM) is proposed to derive IOPs from remote sensing reflectance and to estimate Chl-*a* from the retrieved absorption coefficients. GTM accurately retrieves absorption coefficients at 443 nm and 675 nm with R^2=0.8347 and R^2=0.7541 respectively, although underestimates absorption coefficients at 560 nm with R^2=0.6911. Based on GTM-derived absorption coefficients, the predicted Chl-*a* fits well with laboratory measured Chl-*a* in eight different study sites and in different seasons, and the overall R^2 equals to 0.9292 and mean relative error (MRE) is 21.35%. Thereafter, the models were tested on simulated Medium Resolution Imaging Spectrometer (MERIS) spectra, and both absorption

[*] The manuscript was submitted to Remote Sensing of Environments for review.

coefficients and Chl-*a* concentration were retrieved. Particularly, Chl-*a* was accurately estimated with R^2=0.9138 and MRE=22.78%, which enables possible routine surveillance of Chl-*a* in inland waters using MERIS satellite imagery.

Keywords: globally transferable model, chlorophyll-a, inherent optical properties, MERIS

1. Introduction

1.1 Deriving the inherent optical properties (IOPs)

The underwater light penetration is fundamentally important to aquatic ecosystems because the quantity and quality of underwater light drive the photosynthesis of algae dwelling in water bodies (Gallegos et al., 2005). In-water inherent optical properties (IOPs), including absorption ($a(\lambda)$, *refer to table 2.1 for symbols and abbreviations*) and backscattering ($b_b(\lambda)$) coefficients, are the most significant parameters governing the light propagation within the water column and thus facilitate the estimation of aquatic biomass, primary production, heat flux, and carbon pools (Lee et al., 1996; Le et al., 2009a; Wang et al., 2005; and references therein).

In recent years many efforts have been made to derive the IOPs from the apparent optical properties (AOP) including irradiance reflectance and remote sensing reflectance (e.g. Lee et al., 1996; Le et al., 2009a; Garver & Siegel, 1997; Hoge & Lyon, 1995 & 2005; Wang et al., 2005). Empirical algorithms use simple or multiple regressions to relate the IOPs to the ratio of the AOPs, and can be implemented rapidly, but their application is limited by the variation of optical properties across different water bodies (Le et al., 2009a). Semi-empirical and analytical algorithms based on radiative transfer equations work for different water bodies and usually perform better than the empirical

algorithm. A derivation of IOPs from remote sensing reflectance is commonly based on the reflectance model shown in equation 1 (Gordon et al., 1988) that describes the relationship between remote sensing reflectance and IOPs.

$$r_{rs}(\lambda)=\frac{L_u(0-,\lambda)}{E_d(0-,\lambda)}=g_1\left(\frac{b_b(\lambda)}{a(\lambda)+b_b(\lambda)}\right)+g_2\left(\frac{b_b(\lambda)}{a(\lambda)+b_b(\lambda)}\right)^2 \quad (1)$$

where $r_{rs}(\lambda)$ is the remote sensing reflectance just beneath water surface, $L_u(0\text{-}, \lambda)$ and $E_d(0\text{-}, \lambda)$ are upwelling radiance and downwelling irradiance, respectively, and g_1 and g_2 are geometrical factors. Hereafter the wavelength dependence of all model variables will be omitted for briefness unless it is necessary. Equation 1 is simplified in many studies (e.g., Brando & Dekker, 2003; Giardino et al., 2007; Hoogenboom et al., 1998; Hakvoort et al., 2002; Jupp et al., 1994; Kutser, 2004 & 2006; Zhang et al., 2009) by omitting the quadratic term and resulting in equations 2 and 3:

$$r_{rs}=\frac{f}{Q}\frac{b_b}{a+b_b} \quad (2)$$

$$R(0-)=\frac{E_u(0-)}{E_d(0-)}=f\frac{b_b}{a+b_b} \quad (3)$$

where f is a factor of light field, Q is the light distribution factor defined as $Q=E_u(0-)/L_u(0-)$; $R(0\text{-})$, $E_u(0\text{-})$ and $E_d(0\text{-})$ are subsurface irradiance reflectance, upwelling and downwelling irradiance, respectively.

Build upon equations 2 and 3, several semi-empirical and semi-analytical algorithms have been proposed for deriving the IOPs, including the Garver–Siegel–Maritorena (GSM) algorithm (Garver & Siegel, 1997; Maritorena et al., 2002; Maritorena & Siegel, 2005 & 2006), the algorithm (referred to as HL) by Hoge and Lyon (1996, 1999 & 2005) and the quasi-analytical algorithm (QAA) by Lee et al. (2002, 2004 & 2009). The

difference among them lies in that GSM and HL require pre-defined spectral shapes of phytoplankton absorption ($a_{ph}(\lambda)$) and colored detritus matter (CDM, colored dissolved organic matter (CDOM)+non-algal particles (NAP)) absorption ($a_{cdm}(\lambda)$) while QAA does not have such a requirement.

Table 2.1. Symbols and abbreviations

Symbol/abbreviation	Description	Unit
$L_u(0-)$	Upwelling radiance below water surface	W m^{-2} sr^{-1}
L_x	Radiance. *x* could be *w*: water-leaving radiance; *sw*: total radiance of water surface; *sky*: Sky radiance; *p*: radiance of standard panel	W m^{-2} sr^{-1}
$E_u(0-)$	Upwelling irradiance below water surface	W m^{-2}
E_d	Downwelling irradiance. 0+: above water surface 0-: below water surface	W m^{-2}
$R_{rs}(\lambda)$	Remote sensing reflectance above water surface	sr^{-1}
$r_{rs}(\lambda)$	Remote sensing reflectance below water surface	sr^{-1}
f	Geometrical light factors	-
Q	Light distribution factor	sr
$a(\lambda)$	Total absorption coefficients of water column	m^{-1}
$a_x(\lambda)$	Absorption coefficients of *x*. *x* could be *w*: water; *ph*: *in vivo* phytoplankton; *sol*: *in vitro* phytoplankton; *t-w*: non-water constituents; *cdom*: colored dissolved organic matter; *cdm*: colored detritus matter	m^{-1}
$b_b(\lambda)$	Total backscattering coefficients of water column	m^{-1}
$b_{bx}(\lambda)$	Backscattering coefficients of *x*. *x* could be *w*: water; *p*: suspended particles	m^{-1}
IOPs	Inherent optical properties	m^{-1}
Chl-*a*	Chlorophyll-a (concentration)	mg m^{-3}
TSM	Total suspended matter (concentration)	g m^{-3}
CDOM	Colored dissolved organic matter	-
NAP	Non-algal particles (concentration)	g m^{-3}
CDM	Colored detritus matter, i.e. CDOM+NAP	-

GSM, HL and QAA are originally developed for ocean water and thus may not be suitable for optically complex inland waters due to high concentrations of suspended

sediment (SS) and CDOM (Gons, 1999 & 2000; Schalles et al., 2001; Schalles, 2006; Zhou et al., 2009). Such complexity is primarily manifested in the variation of the factors such as g_1, g_2, f and Q that are used in equations 1, 2 and 3. However, previous studies assume g_1 and g_2 as constants (Garver & Siegel, 1997; Maritorena et al., 2002; Maritorena & Siegel, 2005 & 2006; Hoge & Lyon, 1996, 1999 & 2005; Hoge et al., 1999a & 1999b; Lee et al., 1999, 2002, 2004, 2007 & 2009; Salama et al., 2009; Wang et al., 2005), f or $\frac{f}{Q}$ as a constant (Hoogenboom et al., 1998; Hakvoort et al., 2002), or f as a function of just light geometry (Brando & Dekker, 2003; Giardino et al., 2007; Jupp et al., 1994; Kutser, 2004 & 2006; Zhang et al., 2009). In fact, f, $\frac{f}{Q}$ [g_1 is equivalent to $\frac{f}{Q}$ (Maritorena et al., 2002)] and g_2 depend on many ambient factors including bio-optical states, sun angles, and wind speed (Gould et al., 2001; Morel & Gentilli, 1993 & 1996; Zhang et al., 2009), and as a result may vary sample by sample or across different water bodies (Gould et al., 2001). For example, the values assigned to g_1 and g_2 in QAA (Lee et al., 2002, 2004 & 2009) differ from those in GSM (Garver & Siegel, 1997; Maritorena et al., 2002; Maritorena & Siegel, 2005 & 2006). Although QAA and GSM perform well for many ocean waters using the same set of the algorithm-self-defined g_1 and g_2, the reason for this fact might be due to the relatively homogeneous conditions in ocean waters. In turbid inland water bodies, the variation of these factors is more complex (Zhang et al., 2009), and leads to the dependence of g_1 and g_2 on study locations or sites. Therefore, g_1 and g_2 should be considered as variables, when optically complex inland waters are of interest. The corresponding modification is expected to improve the estimation accuracy of IOPs in inland waters.

1.2 Estimation of chlorophyll-a concentration

Based on accurately retrieved IOPs, especially $a(\lambda)$, many practical applications can be proceeded. One of them is to predict chlorophyll-a (Chl-*a*) concentrations, which is so significant for monitoring increasing algal blooms, especially toxic cyanobacterial blooms (Mathews et al., 2010; Randolph et al., 2008; Simis et al., 2005 & 2007), in reservoirs, lakes and estuaries. Nonetheless, the optical complexity of inland waters makes it difficult to spectrally retrieve Chl-*a* because empirical algorithms for estimating Chl-*a* directly from remote sensing reflectance or leaving water radiance L_w, including band ratio (Dekker, 1993; Gitelson, 1992; Jupp et al., 1994; Kallio et al., 2001; Li et al., 2010), fluorescence line height (Gower & King, 2007; Gons et al., 2008; Hu et al., 2005), three-band tuning algorithms (Dall'Olmo & Gitelson, 2005; Duan et al., 2010; Gitelson et al., 2007, 2008 & 2009), four-band algorithms (Le et al., 2009b & 2010) and other band combination methods (Budd et al., 2004; O'Reilly et al., 1998), are usually limited to the dataset on which they are calibrated (Giardino et al., 2007; Matthews et al., 2010). Particularly, when SS concentration is high, the scattering of SS usually masks the optical response of Chl-*a*, reducing the predictive power of the empirical algorithm (Bukata et al., 1995; Zhou et al., 2009). Therefore, IOCCG (2006) and Zhou et al. (2009) suggested to derive Chl-*a* from IOPs for highly turbid inland waters rather than to derive directly from AOPs. Fortunately, several equations, e.g., equations developed by Ritchie (2008), can be used to quantify Chl-*a* from *in vitro* $a_{ph}(\lambda)$ in laboratory and have potential to be applied on predicted *in vivo* $a_{ph}(\lambda)$ with slight modification. In addition, Chl-*a* concentration could be simply determined by dividing its specific absorption coefficient, i.e. absorption per unit Chl-*a*, at 665 nm ($a^*_{ph}(665)$) from total *in vivo* $a_{ph}(665)$, because $a^*_{ph}(665)$

should be stable through inland waters. The stability of $a^*_{ph}(665)$ is proved by the fact that Gons (1999) and Gons et al. (2000, 2002 & 2008) observed that $a^*_{ph}(665) \approx 0.016$ m^2 (mg Chl-*a*)$^{-1}$ works for tens of sites in Netherlands, Lake Chao and Tai in China, Hudson/Raritan Estuary of New Jersey and New York and the Great Lakes in USA, etc.

1.3 Objectives of this study

The primary aim of this study is to establish a globally transferable model (GTM) that could be used to invert the IOPs from remote sensing reflectance and then to estimate Chl-*a* concentration from the retrieved IOPs of inland waters. The developed model should derive IOPs without requiring a pre-defined shape of the specific absorption spectrum of an individual constituent, and are transferable across different sites and different seasons for quantifying Chl-*a* from retrieved *in vivo* absorption coefficients.

2. Data collection

The datasets used in this study were collected by different research groups, and the procedures for field water sampling, *in situ* spectral measurements and laboratory analysis for pigment concentration are not identical. The descriptive statistics of field measurements and laboratory analysis results are shown in Fig. 2.1, Fig. 2.2 and table 2.2.

2.1 Study sites

Lake Tai, China. Lake Taihu (LT) (30^o 56'–31^o 33' N, 119^o 55.3'–120^o 53.6' E), the third largest freshwater lake in China, locates in the south of Yangtze River Delta. The total area of the lake is 2338 km^2, with an average water depth of 1.9 m and a total water capacity of 47.6×10^8 m^3 (Le et al., 2009b). The water quality is severely deteriorated because of the increased discharge of wastewater, sewage and polluted water resulted from rapid economic development in the surrounding urban and rural regions. Algal

blooms frequently occur in some sub-regions, and the sediment resuspension is strong resulted from wave effects. Thus, Lake Tai is thought to be a typical highly turbid eutrophic lake (Sun et al., 2010).

Shitoukoumen Reservoir, China. Shitoukoumen Reservoir (SR) (43^{o} 54.6' N, 125^{o} 46.95' E) is the major water sources for Changchun and Jiutai County, in the Jilin province of Northeast China, which provide more than 80% of the drinking water for the Changchun City (Lu et al., 2010). It has storage capacity of 70.2×10^{7} m^{3}, drainage area of 4975.6 km^{2} and surface area of 94.2 km^{2} respectively (Xu et al., 2009). It is situated in north temperate sub-humid continental monsoon climate zone, with the mean annual temperature 5.3 ^{o}C and precipitation range from 369.9 to 667.9 mm. In recent years, serious soil erosion and water loss in the upstream increased nutrient input to the reservoir, and the eutrophication status is drawing intense attention from environmental agency and water supplying company.

Sites in Australia. Myponga Reservoir (35^{o} 23.7’ S, 138^{o} 26.5’ E), about 70 km south from Adelaide, provides nearly 5% of water supply for Adelaide. It has a storage capacity of 26.8×10^{6} m^{3} with surface area about 2.8 km^{2} and the average depth about 15 m with maximum as 36 m. River Murray starts from the Snowy Mountains in the eastern highlands and flows for 2560 km until entering to ocean via Lake Alexandrina in South Australia (Baker et al., 2000). Lower River Murray is the major source for irrigation and drinking water in South Australia (Maier et al., 1998; Burch et al., 1994). In our study, River Murray at Mannum and Wellington were selected as study areas. River Murray at Mannum (34^{o} 54.8' S, 139^{o} 18.9' E), about 100 km east from Adelaide, is about 150 km

upstream of the Murray Mouth. River Murray at Wellington (35° 20.3' S, 139° 23.3' E) is close to Murray Mouth where Murray River merges into Lake Alexandrina.

Sites in Indiana, USA. The study sites are three central Indiana reservoirs, Eagle Creek Reservoir (39°51' N, 86°18.3' W), Geist Reservoir (39°55' N, 85°56.7' W) and Morse Reservoir (40°6.4' N, 86°2.3' W). The three reservoirs have similar depth (3.2-4.7 m), surface area (5-7.5 km^2), volume (21-28×10^6 m^3) and residence time (55-70 days). They were selected as the study sites because of their importance of supplying drinking water for residents surrounding Indianapolis metropolitan area, and that they all face the serious eutrophication problem.

2.2 Remote sensing reflectance measurements

ASD field spectrometer (Analytical Spectral Devices, Inc., Boulder, CO, USA) was used to measure remote sensing reflectance above water surface, denoted as $R_{rs}(\lambda)$, on Lake Tai in both 2006 and 2007 and on Shitoukoumen Reservoir from 2006 to 2008. The measurements followed the Ocean Optical Protocols by NASA (Revision 3; Muerller & Fargion, 2002). Radiance of water (L_{sw}), sky (L_{sky}) and reference panel (L_p) were measured several times at each sample station to eliminate the error due to inappropriate operation. When measuring L_{sw}, an 1.5 m-long extending pole was positioned about 1 m above water surface with azimuth angle from sun as ~135° and zenith angle as ~45° to minimize the shading and sunglint effects (Mobley, 1999), and L_{sky} was measured in the same plane but by rotating the pole upward ~90°. R_{rs} was then computed as:

$$R_{rs} = \frac{L_w}{E_d(0+)} = \frac{L_{sw} - rL_{sky}}{E_d(0+)} \quad (4)$$

where L_w is the water-leaving radiance, r represents the reflectance of the skylight from air-water interface (Mobley, 1999), and $E_d(0+)$ is the downwelling irradiance above water surface and defined as:

$$E_d(0+) = \frac{\pi L_p}{\rho_p} \tag{5}$$

where ρ_p stands for the reflectance of reference panel, and it has been calibrated as 30% in our case.

Ocean Optics USB4000 (Ocean Optics, Inc., Dunedin, FL, USA) with dual radiometers was used to measure below water surface remote sensing reflectance $r_{rs}(\lambda)$ on Indiana three central reservoirs in 2008 and 2010, and on Australian study sites in 2009. Reflectance spectra were measured by following the procedure described in Gitelson et al. (2008). Radiometer 1 was pointed upward by mounting on a 2 m high pole to measure the real-time incidence irradiance ($E_d(0+)$). Simultaneously, radiometer 2, equipped with a 25^o field-of-view optical fiber, was dipped ~2 cm into water surface with a 2 m-long pole and pointed downward to measure the below-surface upwelling radiance ($L_u(0-)$) at nadir. Back to laboratory, the spectra collected *in situ* were processed using software CDAP/CALMIT (University of Nebraska at Lincoln) and r_{rs}' is computed:

$$r_{rs}' = \frac{L_u(0-)}{E_d(0+)} \tag{6}$$

Morel and Maritorena (2001) stated $E_d(0-)=0.965E_d(0+)$, therefore, r_{rs} can be finally computed as:

$$r_{rs} = \frac{r_{rs}'}{0.965} \tag{7}$$

Table 2.2. The sampling date, number of samples and ranges of measured Chl-*a* and TSM as well as absorption and backscattering parameters

Site	**Date**	***N***	**Chl-*a*** mg m^{-3}	**TSM** g m^{-3}	a_{cdom}**(440)** m^{-1}	a_{t-w}**(440)** [a] m^{-1}	a_{t-w}**(675)** [a] m^{-1}	b_{bp}**(560)** [b] m^{-1}	**Y** [b] -
LT in China	Oct.-Nov. 2006 & Nov. 2007	62[c]	2.54-246.61	6.47-143.47	-	0.51-15.75	0.085-3.83	0.20-5.33	0.19-0.72
SR in China	Apr. 2006 - Sep. 2008	119	1.87-47.52	3.67-211.91	-	0.64-13.03	0.025-1.05	0.13-8.02	0.34-0.79
Sites in Australia	Feb. 2009 - Mar. 2009	60	6.58-79.41	2.00-94.00	-	1.37-13.04	0.072-2.17	0.03-1.52	-0.19-0.27
Sites in Indiana	Jul. 2008 - Nov. 2008	64	25.40-285.80	1.51-33.77	-	1.00-5.68	0.439-3.87	0.13-3.72	0.29-0.91
	Apr. 2010 - Oct. 2010	191	1.85-129.39	5.17-81.17	0.48-3.81	0.73-7.83 (1.26-6.95)	0.037-2.51 (0.215-2.41)	0.07-1.10	-0.10-0.91

[a] Only samples collected in Indiana 2010 were analyzed for these parameters and the measured values are shown in parenthesis. Values estimated from GTM for all sites and years are also listed here for demonstrating the variations among the sites.

[b] All values comes from GTM-estimated results and listed here for comparison purpose.

[c] 17 samples were excluded for statistical analysis and model test because of the presence of algal scums.

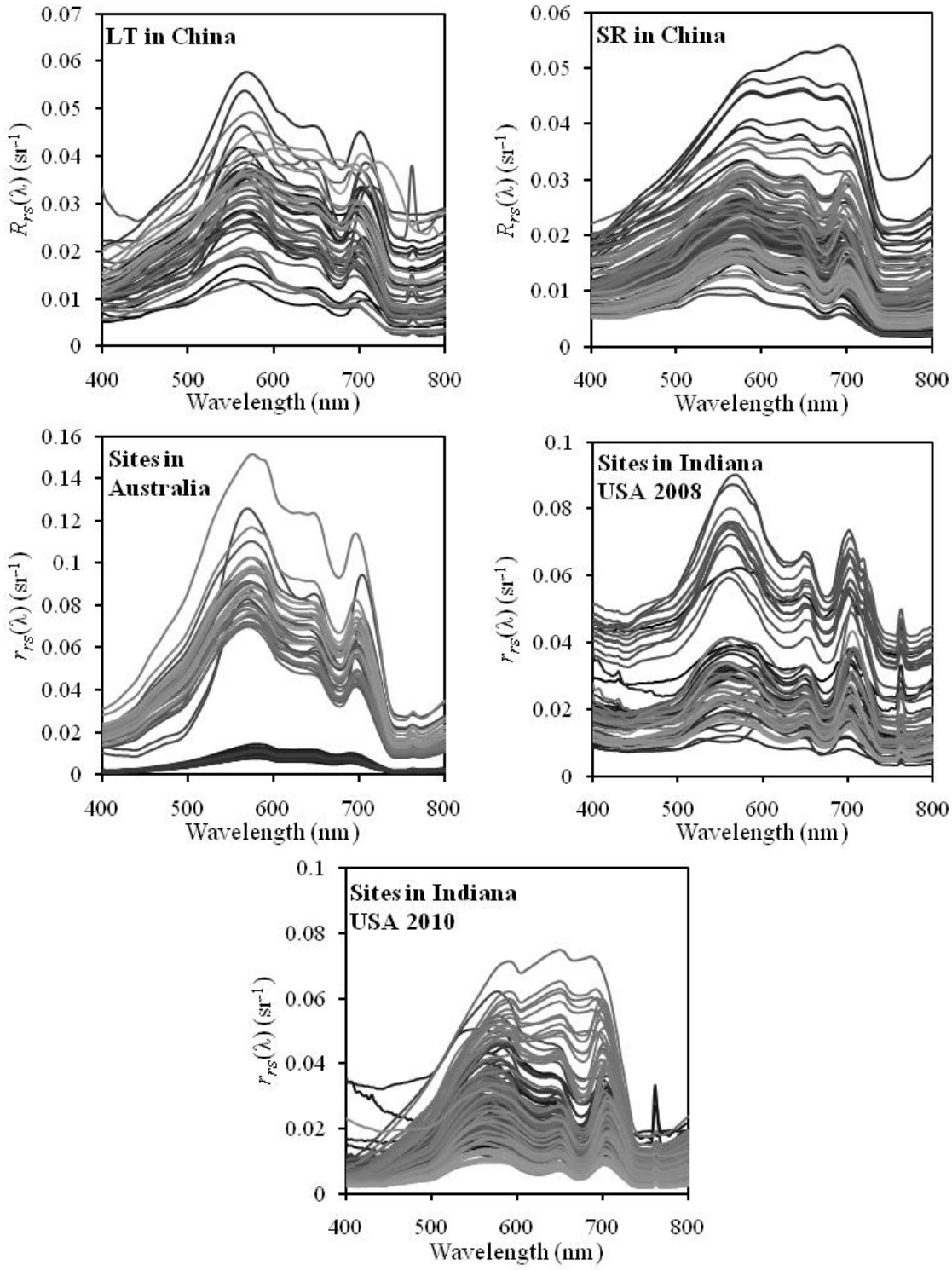

Fig. 2.1. Above ($R_{rs}(\lambda)$) and below ($r_{rs}(\lambda)$) surface remote sensing reflectance spectra measured instudy sites.

2.3 Chl-a and total suspended matter concentration measurements

Water samples collected in all sites were put in cold and dark coolers and then transported back to laboratory for Chl-*a* and total suspended matter (TSM) concentration measurements.

Water samples for Chl-*a* extraction passed 0.45 μm pore size GF/C filters (Whatman), after which Chl-*a* was extracted with 90% ethanol at 80 ^{o}C and 90% acetone for samples collected at LT and SR, respectively. Then optical density of Chl-*a* extracts was measured using spectrophotometer and Chl-*a* was calculated according to Lorenzen (1967). For samples collected in three central Indiana reservoirs, 2008 and those collected in Australia, the measurements followed the procedure by EPA Method 445.0 (Arar & Collins, 1997) and Randolph et al. (2008). Chl-*a* extraction samples passed 0.45 μm pore size acetate filters (Whatman) and were extracted in 90% acetone, and then Chl-*a* was measured by a pre-calibrated TD-700 fluorometer (Turner Designs, Inc., Sunnyvale, CA, USA). Thereafter, for samples collected in three sites of Indiana, 2010, 0.45 μm pore size acetate filter (Whatman) and 90% acetone were used as the extraction material and reagent, but Chl-*a* was determined from absorption coefficients ($a_{sol}(\lambda)$, referred as *in vitro* $a_{ph}(\lambda)$; shown in Fig. 2.3) measured by spectrophotometer based on equation given by Ritchie (2008).

TSM concentration was determined gravimetrically. According to the turbidity of samples, 150-300 ml of water sample was filtered onto pre-ashed (530 ^{o}C for 1.5 hours for samples of Indiana and 4 hours for other samples, respectively), pre-filtered (200 ml Milli-Q water) and pre-weighed GF/F filters (Whatman). Subsequently, the filters with particles were dried at 105 ^{o}C (1.5 hours for samples of Indiana and 4 hours for other

samples, respectively) and weighted with an electronic balance to obtain the TSM concentration.

2.4 Absorption coefficients measurements

Absorption of water constituents except water itself ($a_{t\text{-}w}(\lambda)$) and absorption of CDOM ($a_{cdom}(\lambda)$) were measured for samples collected in Indiana sites, 2010. The unfiltered water samples was poured into 1-cm cuvette and scanned by spectrophotometer (380-800 nm, 1 nm resolution) with Milli-Q water as reference, and its optical density ($OD_{t\text{-}w}(\lambda)$) was determined for each sample except the first forty samples collected in April and May, 2010. Similarly, $OD_{cdom}(\lambda)$ was measured using the same instrument and configuration, but pre-filtered samples that passed 0.22 μm pore size GF/F filters (Whatman) were used. Subsequently, the average of $OD_{t\text{-}w}(\lambda)$ between 750 nm and 800 nm was subtracted from $OD_{t\text{-}w}(\lambda)$ for correcting backscattering effect, when $OD_{cdom}(\lambda)$ was corrected for this effect according to Bricaud et al. (1981) and Zhang et al. (2009). Finally, $a_{t\text{-}w}(\lambda)$ and $a_{cdom}(\lambda)$ were computed based on:

$$a_x(\lambda) = 2.303 OD_x(\lambda)/l \tag{8}$$

where x represents either *t-w* or *cdom*, 2.303 is used to convert 10-based log to natural log and l (=0.01 m) is optical pathlength. Both absorption spectra were then smoothed in MATLAB (MathWorks, Inc., Natick, MA, USA) using spline function.

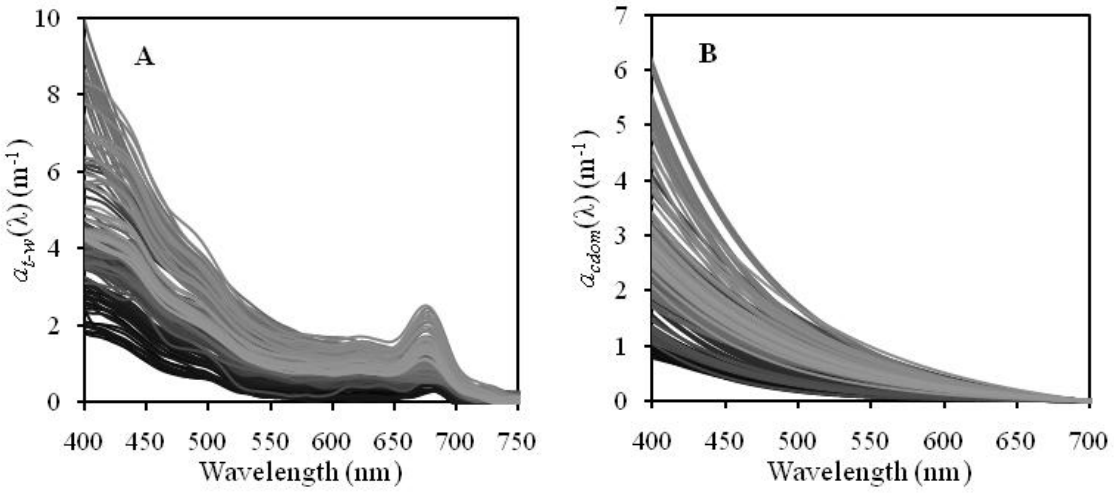

Fig. 2.2. A: measured $a_{t\text{-}w}(\lambda)$; B: measured $a_{cdom}(\lambda)$. Both $a_{t\text{-}w}(\lambda)$ and $a_{cdom}(\lambda)$ are only available for samples collected in Indiana sites 2010, and 40 samples were dumped because of inappropriate storage.

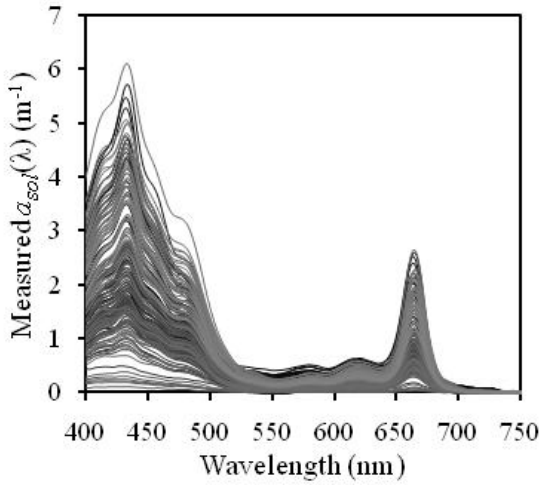

Fig. 2.3. Measured $a_{sol}(\lambda)$ of samples collected in Indiana 2010. $a_{sol}(\lambda)$ is also referred as *in vitro* $a_{ph}(\lambda)$.

3. Model for IOPs inversion

The derivation of the IOPs from remote sensing reflectance starts with a reflectance ratio. Although f or Q depends on the factors including bio-optical states, sun angles, wind speed as well as on wavelength (Morel & Gentili, 1993 & 1996) for a given sample

location, f/Q has a weak dependence on wavelength. Based on equation 2, the reflectance ratio can be written as:

$$\frac{R_x(\lambda_1)}{R_x(\lambda_2)}=\frac{b_b(\lambda_1)[a(\lambda_2)+b_b(\lambda_2)]}{b_b(\lambda_2)[a(\lambda_1)+b_b(\lambda_1)]} \tag{9}$$

where $R_x(\lambda)$ can be either $r_{rs}(\lambda)$ or $R_{rs}(\lambda)$ because they are linearly correlated as shown in equation 10 (Doxaran et al., 2002; Salama et al., 2009).

$$R_{rs}(\lambda)=\frac{t_-t_+}{n^2}r_{rs}(\lambda) \tag{10}$$

where t_- and t_+ are the transmittance factor of light from water to air and from air to water, respectively, and n is the refractive index of water. The value of $\frac{t_-t_+}{n^2}$ is commonly set to 0.54.

To reduce unknowns in equation 10, λ_2 is selected to be a wavelength longer than 700 nm where the absorption of water constituents is negligible and total absorption coefficient is approximated by the absorption of water ($a_w(\lambda)$), i.e. $a(\lambda_2)\approx a_w(\lambda_2)$ (Gons, 1999 & 2000; Gons et al., 2005; Simis et al., 2005 & 2007; Gould et al., 2001; Le et al., 2009a). Based on this assumption, Gons (2005) calculated $b_b(778)$ from remote sensing reflectance using equation 11 because $a_w(\lambda)$ is invariant with temperature around 780 nm (Salama et al., 2009) and the value for $a_w(\lambda)$ was adopted from Buiteveld et al. (1994).

$$b_b(778)=\frac{r_{rs}(778)a_w(778)}{0.082-r_{rs}(778)} \tag{11}$$

$b_b(\lambda)$ and backscattering coefficients of particles ($b_{bp}(\lambda)$) could be expressed as equation 12 and equation 13 respectively (Lee et al., 2002, 2004 & 2009).

$$b_b(\lambda)=b_{bp}(\lambda)+b_{bw}(\lambda)=b_{bp}(560)\left(\frac{560}{\lambda}\right)^{Y}+b_{bw}(\lambda) \tag{12}$$

$$b_{bp}(560)=\frac{b_b(778)-b_{bw}(778)}{(560/778)^{Y}} \tag{13}$$

where $b_{bw}(\lambda)$ represents the backscattering coefficient of water (Buiteveld et al., 1994); Y is a constant for a given $b_b(\lambda)$ and can be derived from the reflectance ratio of band 443 nm to band 560 nm as shown in equation 14 (Lee et al., 2009). Equation 15 (Lee et al., 2002, 2004 & 2009) is used to calculate under surface remote sensing reflectance if above surface remote sensing reflectance is available.

$$Y=2.0\left[1-1.2\exp\left(-0.9\frac{r_{rs}(443)}{r_{rs}(560)}\right)\right] \tag{14}$$

$$r_{rs}(\lambda)=\frac{R_{rs}(\lambda)}{0.52+1.7R_{rs}(\lambda)} \tag{15}$$

After $b_b(\lambda)$ at all wavelengths is estimated using equations 11-15 and λ_2 in equation 9 is appropriately specified, the total absorption could be calculated by solving equation 9. Simis et al. (2005 & 2007) suggested that a wavelength around 709 nm is suitable for λ_2. Therefore, $a_{t\text{-}w}(\lambda)$ is computed using equation 16.

$$a_{t-w}(\lambda)=\frac{R_x(709)b_b(\lambda)[a_w(709)+b_b(709)]}{R_x(\lambda)b_b(709)}-b_b(\lambda)-a_w(\lambda) \tag{16}$$

$a_w(\lambda)$ changes with temperature, especially it fluctuates apparently at wavelengths around 750 nm (Buiteveld et al., 1994; Gould et al., 2001), and $a_w(\lambda)$ measured at 20 ^{o}C by Buiteveld et al. (1994) was adopted because 20 ^{o}C is the average temperature observed in Indiana study sites 2010. This $a_w(\lambda)$ is suitable for most of study sites, for its change with temperature is not significant, at least for wavelength shorter than 715 nm.

4. Model for Chl-*a* retrieval

The derived non-water constituent bulk absorption (equation 16) should be related to the phytoplankton absorption in order to estimate Chl-*a*. Assuming that the CDM absorption is negligible at wavelengths longer than 620 nm, i.e. $a_{ph}(\lambda) \approx a_{t\text{-}w}(\lambda)$ for $\lambda \geq 620$ nm, Simis et al. (2005 & 2007) proposed an empirical relationship to convert the non-water bulk absorption to *in vitro* phytoplankton absorption at 665 nm ($a_{sol}(665)$):

$$a_{sol}(665) = \frac{a_{t-w}(665)}{0.68} = \frac{a_{ph}(665)}{0.68} \tag{17}$$

Simis et al. (2007) suggested that 0.68 is used in equation 17 to compensate the weak signal received by remote sensing instrument relative to that measured by a lab spectrophotometer. In this study, this constant is interpreted to correct the package effect and band shift between $a_{sol}(\lambda)$ and $a_{ph}(\lambda)$ (see section 5.3.1) when conversion $a_{t\text{-}w}(665)$ to $a_{sol}(\lambda)$ is required for application of equation 18 (Ritchie, 2008). Note that in equation 18 the unit is converted to mg m^{-3} from g m^{-3}, and the effect of optical pathlength (=0.01 m) is corrected.

$$\begin{aligned} \text{Chl}-a\ (\text{mg m}^{-3}) = [&-0.3319 a_{sol}(630) - 1.7485 a_{sol}(647) \\ &+ 11.9442 a_{sol}(665) - 1.4306 a_{sol}(691)] \times 4.34 \end{aligned} \tag{18}$$

The absorption coefficients at 630 nm, 647 nm and 691 nm are small and the package effects are also weak, thus it is valid to assume that $a_{sol}(\lambda_i)$ (λ_1=630, λ_2=647 and λ_3=691) approximately equals to $a_{t\text{-}w}(\lambda_i)$ and to use equation 18 for Chl-*a* estimation from $a_{t\text{-}w}(\lambda_i)$.

While Ritchie's Chl-*a* model is modified for *in vivo* phytoplankton absorption case, it requires four bands. For purpose of estimating Chl-*a* only, an alternative could be pursued as shown in equation 19:

$$\text{Chl}-a(\text{mg m}^{-3}) = \frac{a_{ph}(665)}{a^*_{ph}(665)} \approx \frac{a_{t-w}(665)}{a^*_{ph}(665)} \tag{19}$$

where $a^*_{ph}(665)$ denotes the specific absorption of phytoplankton at 665 nm and is set to be 0.016 m^2 (mg Chl-*a*)$^{-1}$ (Gons et al., 2008).

Table 2.3. Globally transferable model (GTM) for deriving the inherent optical properties (IOPs) and Chl-*a* concentration

Step	Variable	Formula
1	$b_b(778)$	$b_b(778) = \frac{r_{rs}(778)a_w(778)}{0.082 - r_{rs}(778)}$
2	Y	$\text{Y} = 2.0\left[1 - 1.2\exp\left(-0.9\frac{r_{rs}(443)}{r_{rs}(560)}\right)\right]$ If necessary, $r_{rs}(\lambda) = \frac{R_{rs}(\lambda)}{0.52 + 1.7R_{rs}(\lambda)}$
3	$b_{bp}(560)$	$b_{bp}(560) = \frac{b_b(778) - b_{bw}(778)}{0.7198^{\text{Y}}}$
4	$b_b(\lambda)$	$b_b(\lambda) = b_{bp}(560)\left(\frac{560}{\lambda}\right)^{\text{Y}} + b_{bw}(\lambda)$
5	$a_{t\text{-}w}(\lambda)$	$a_{t-w}(\lambda) = \frac{R_x(709)b_b(\lambda)[a_w(709) + b_b(709)]}{R_x(\lambda)b_b(709)} - b_b(\lambda) - a_w(\lambda)$ where $R_x(\lambda)$ represents either $R_{rs}(\lambda)$ or $r_{rs}(\lambda)$
6	Chl-*a* (mg m^{-3})	$\text{Chl}-a = [-0.3319a_{sol}(630) - 1.7485a_{sol}(647) + 11.9442a_{sol}(665) - 1.4306a_{sol}(691)] \times 4.34$ where $a_{sol}(665) = \frac{a_{t-w}(665)}{0.68}$ and $a_{sol}(\lambda_i) = a_{t-w}(\lambda_i)$ (λ_i = 630, 647 and 691, respectively)
	Chl-*a* (mg m^{-3})	$\text{Chl}-a = \frac{a_{t-w}(665)}{a^*_{ph}(665)}$, $a^*_{ph}(665) = 0.016$ m^2 (mg Chl-*a*)$^{-1}$

Steps of GTM above are summerized in table 2.3 and the GTM-estimated Chl-*a* accuracy is evaluated using root mean square error (RMSE), relative error (RE) and mean relative error (MRE) are used in this paper, and their definitions are shown in equation 20, equation 21 and equation 22, respectively.

$$\mathrm{RMSE}=\sqrt{\frac{1}{N}\sum_{i=1}^{N}(X'-X)^2} \tag{20}$$

$$\mathrm{RE}(\%)=\frac{|X'-X|}{X}\times 100\% \tag{21}$$

$$\mathrm{MRE}(\%)=\frac{1}{N}\sum_{i=1}^{N}RE_i \tag{22}$$

where X' is estimated value, X is measured value and N is sample number.

5. Results and discussion

5.1 Derived Absorption Coefficient

The estimated $a_{t\text{-}w}(\lambda)$ spectra corresponding to the highest and lowest Chl-*a* at the study sites are shown in Fig. 2.4.A. The shape of these estimated $a_{t\text{-}w}(\lambda)$ spectra can be divided into three groups: 1) the spectra in the first group are dominated by phytoplankton absorption (e.g., Aus-MAX) and show distinctive pigment absorption features at 443 and 675 nm due to Chl-*a* and at 490 nm due to carotenoid; 2) the spectra included in the second group show the absorption characterized by both phytoplankton and CDM (e.g. IN10-MAX), i.e. the pigments absorption features are distinctive but superimposed on the CDM absorption at short wavelengths; 3) the third group spectra (e.g. IN10-MIN) exhibit the characteristic CDM absorption, i.e. exponential decay curves without distinctive pigment absorption peaks. This qualitative evaluation implies that GTM works for water bodies with different constituent compositions, but not only for waters dominated by a single constituent. A quantitative comparison between GTM-estimated $a_{t\text{-}w}(\lambda)$ and measured $a_{t\text{-}w}(\lambda)$ is made for spectral bands 443, 675 and 550 nm to assess the accuracy of the derived absorption spectra. The comparisons for bands 443 and 675 nm are shown in Fig. 2.4.B and Fig. 2.4.C, respectively. Among all samples, the

highest $a_{ph}(675)$ equals to 3.87 m^{-1} and lowest $a_{ph}(675)$ equals to 0.025 m^{-1}; correspondingly the highest $a_{t\text{-}w}(443)$ is 15.75 m^{-1} and the lowest $a_{t\text{-}w}(443)$ is 0.51 m^{-1}. For band 443 nm, a high correlation between GTM-estimated and measured absorption coefficients was obtained with R^2=0.8347, while for band 675 nm a slightly low correlation was yielded underestimated with R^2=0.7541. Both qualitative and quantitative analyses indicate that GTM can be used for derivation of the non-water absorption coefficient of inland water bodies.

However, a similar comparison made for band 560 nm indicates that GTM underestimated the absorption (Fig. 2.4.D). The underestimation possibly results from dropping the quadratic term of equation 1 when GTM was derived. Generally, $a(560)$ is relatively low and $b_b(560)$ is high, resulting in that $\frac{b_b(560)}{a(560)+b_b(560)}$ is often higher than 0.2. Dropping the quadratic term of equation 1 in the GTM development is expected to result in an overestimated $\frac{b_b(560)}{a(560)+b_b(560)}$ by at least 15% (Garver & Siegel, 1997). This overestimation in turn induces underestimated $a(560)$ by at least 17% if $b_b(560)$ is correctly estimated. Therefore, the quadratic term of equation 1 is critical in order to improve the GTM performance in estimating $a_{t\text{-}w}(560)$ from high reflectance spectra of turbid waters, and such an improvement on GTM needs to determine g_2 for each sample location.

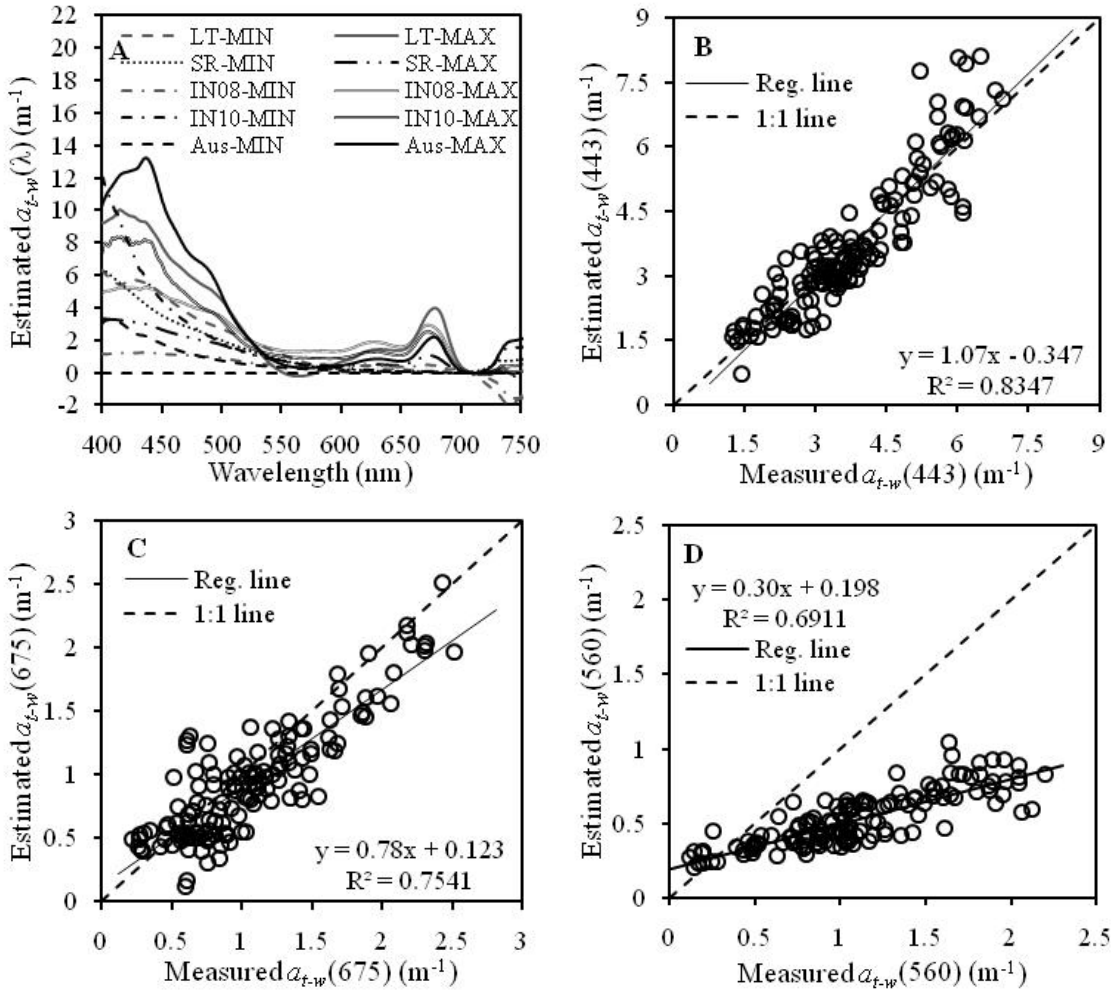

Fig. 2.4. A: GTM-estimated $a_{t\text{-}w}(\lambda)$ vs. wavelength for samples with highest and lowest Chl-*a* at each site. IN08 = Indiana 2008; IN10 = Indiana 2010; Aus = Australia. MIN means minimal Chl-*a* and MAX means maximal Chl-*a*; B, C and D: GTM-estimated $a_{t\text{-}w}(\lambda)$ vs. measured $a_{t\text{-}w}(\lambda)$ for featured bands.

Given the weakness of GTM developed in this study, it is interesting to compare the GTM performance relative to other similar algorithms described in the literature. QAA (version 5; Lee et al., 2009) was selected for the comparison purpose with the samples collected in Indiana, 2010 for which the measured absorption coefficient is available. QAA was chosen because of its simplicity relative to GSM and HL that require pre-

defined absorption spectral shapes of individual constituents. It starts from empirically estimated $a_{t\text{-}w}(560)$ which is then used to calculate the absorption of other wavelengths. The absorption spectra derived with QAA are shown in Fig. 2.5.A, and comparison between QAA-derived and measured absorption coefficients are shown in Fig. 2.5.B for band 443 nm, Fig. 2.5.C for band 675 nm and Fig. 2.5.D for band 560 nm. All R^2 values for QAA are smaller than those for the GTM results, and significantly underestimated $a_{t\text{-}w}(560)$ is observed in the QAA result. Underestimated $a_{t\text{-}w}(560)$ in the QAA result might result from using the fixed g_1 and g_2 for all sample locations and from using the simple empirical equation linking $a_{t\text{-}w}(560)$ to $\log\{[r_{rs}(443)+r_{rs}(490)]/[r_{rs}(560)+5\times\frac{r_{rs}(667)}{r_{rs}(490)}\times r_{rs}(667)]\}$. Underestimation for the absorption coefficients at bands 443 and 675 nm by QAA is also rooted in underestimated $a_{t\text{-}w}(560)$, and this is a major limitation of QAA in estimating the absorption for application to reflectance spectra of optically complex inland waters unless a calibration similar to what Le et al. (2009) did for Lake Tai is made. In contrast, GTM overcomes some limitations and does not need the calibration process even for a water body as complex as Lake Tai, and this conclusion is supported by the correlation between measured Chl-*a* concentration and those estimated with the GTM derived absorption spectra for Lake Tai water samples.

The absorption spectra derived by both GTM and QAA show anomalies beyond 715 nm where $a_{t\text{-}w}(\lambda)$ should approach to zero. The anomaly can be partially contributed to the temperature effect on $a_w(\lambda)$ around 750 nm (Gould et al., 2001) because the correction for his effect was not done on a site basis but used the absorption of water at 20°C for all samples. Nonetheless, the increase of $a_w(\lambda)$ due to temperature cannot explain such big

errors (up to ±2 m^{-1}) in the derived absorption coefficient, and additional research efforts are necessary to figure out the exact reason for this.

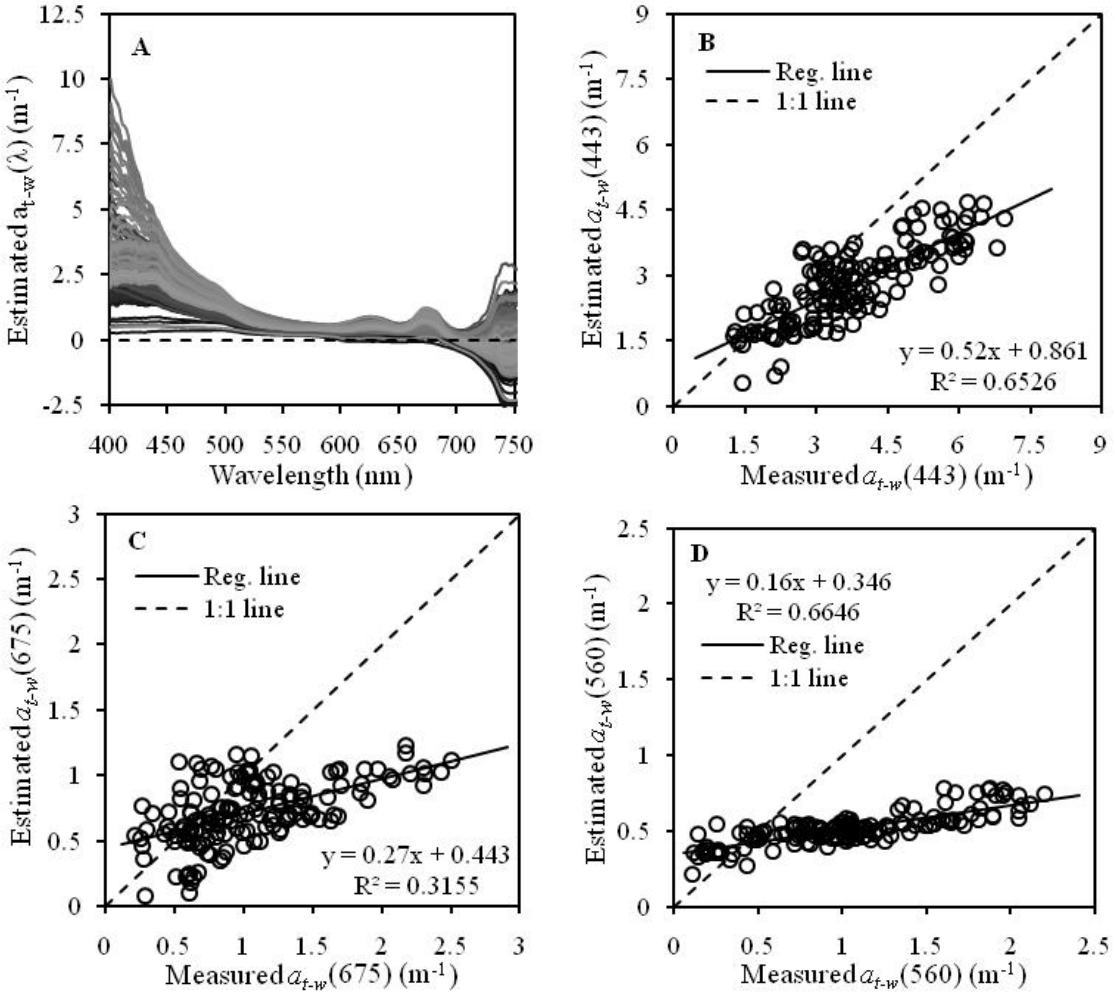

Fig. 2.5. A: Comparison between estimated $a_{t-w}(\lambda)$ using QAA and measured $a_{t-w}(\lambda)$ for smaples collected in Indiana sites 2010; B, C, D: QAA-estimated $a_{t-w}(\lambda)$ vs. wavelength for featured bands.

5.2 Backscattering

Shown in table 2.2 and Fig. 2.6 are the the ranges of GTM-estimated $b_{bp}(560)$ and estimated Y with equation 14. While no measured backscattering cofficients are available for validating estimated values, a meaningful analysis could still be made. For example,

the highest $b_{bp}(\lambda)$ was derived for SR, China and the lowest for Myponga Reservoir, Australia. This reflects the difference of turbidity between these two sites, i.e. SR owns the most turbid water and water in Myponga Reservoir is the clearest. The power Y also shows variability among sites and seasons, but most of Y values are within the range of 0-1 which is typical for case 2 waters (Sathyendranath & Prieur, 1989). Negative Y values are present for phytoplankton dominated water samples and attributed to the strong absorption of phytoplankton that makes $b_{bp}(\lambda)$ at 412-488 nm lower than $b_{bp}(\lambda)$ at longer wavelength (Gallegos et al., 2005). In addition, the variability of Y could also be due to the biochemical difference of particles, e.g. a high Y value implies the dominance of small plankton or mineral particulate (Gallegos et al., 2005).

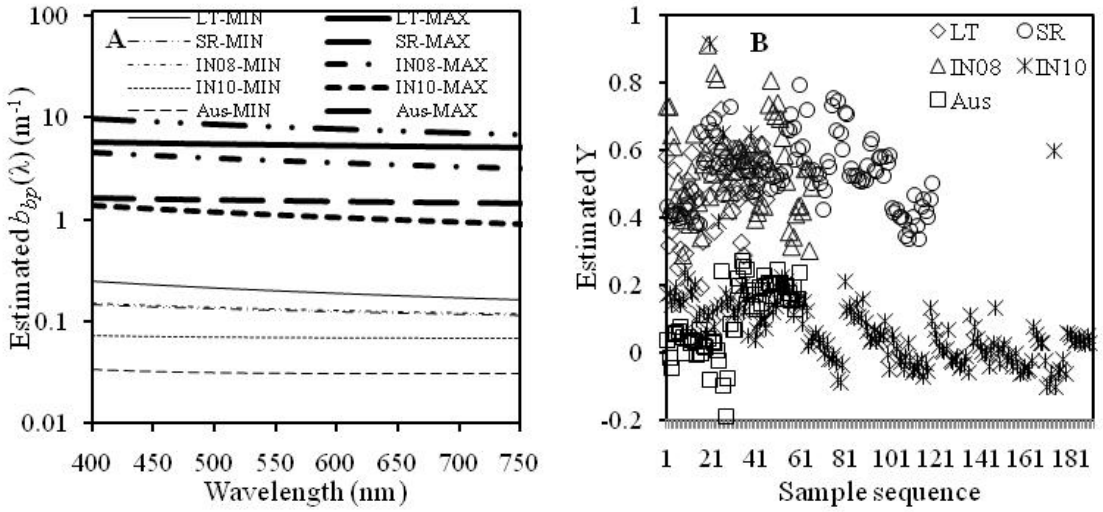

Fig. 2.6. GTM-estimated backscattering coefficients. A: the maximal (MAX) and minimal (MIN) $b_{bp}(\lambda)$ for the sites including Indiana (IN08 & IN10), Lake Tai (LT) and Shitokoumen (SR) in China, and Australia (AU); B: variability of estimated Y for each site.

5.3 Chlorophylls

5.3.1 Chlorophylls estimation

Equations 18 was first applied to the GTM derived absorption coefficients for estimating Chl-*a*. The correlation between estimated and measured Chl-*a* concentration is shown in Fig. 2.7 and the estimation accuracy is listed in table 2.4. The estimation accuracy for all 477 samples is reflected by R^2=0.9232, RMSE=13.0704 mg m^{-3} and MRE=21.25%, respectively, indicating that Chl-*a* is reliabley estimated for samples collected from the study sites over the world and in seasons and that the GTM derived absorption coefficients are accurate enough for estimation of Chl-*a* concentration for the investigated water bodies. However, when considering the performance of equation 18 for individual sites, the lowest R^2 (=0.7938) is observed for SR, and for LT both RMSE (=29.0668 mg m^{-3}) and MRE (=28.28%) are the highest. These two water bodies, compared to other water bodies with high R^2 and low MRE, are the most turbid with more NAP among eight investigated, implying estimated Chl-*a* for highly turbid waters is not as accurate as those for the phytoplankton dominated water. Nevertheless, the estimation accuracy for both SR and LT are still satisfactory.

As stated above, to estimate Chl-*a* with equation 18, the GTM-estimated *in vivo* $a_{ph}(665)$ should be converted to $a_{sol}(665)$ first, while this coversion is not required for bands 630, 647 and 691 nm due to very weak package effects. Equation 17 is currently used for such conversion. While equation 17 is the same as that by Simis et al. (2005 & 2007), the interpretation proposed in this study differs from that by Simis et al. (2005&2007) who suggested 0.68 was used to compensate weaker signal received by remote sensors and here we suggest that constant 0.68 could be used to correct package

effects and a band shift existing between *in vivo* and *in vitro* phytoplankton absorption coefficients. This is supported by the relationship between the GTM-estimated *in vivo* $a_{ph}(665)$ and $a_{sol}(665)$ with a slope of 0.69 shown in Fig. 2.8, very close to 0.68 used in equation 17.

Table 2.4. Evaluation of Chl-*a* estimation from GTM-estimated $a_{t\text{-}w}(\lambda)$ using equation 18 and equation 19. LT=Lake Tai, SR=Shitoukoumen Reservoir, Aus=Sites in Australia, IN08=Sites in Indiana 2008, IN10=Sites in Indiana 2010.

Site	Slope		Intercept		R^2		RMSE (mg m^{-3})		MRE(%)	
	Eq. 18	Eq. 19	Eq. 18	Eq. 19	Eq. 18	Eq. 19	Eq. 18	Eq. 19	Eq. 18	Eq. 19
LT	1.193	1.1239	-1.3229	-1.451	0.9693	0.9695	29.0668	27.2695	28.28	28.07
SR	0.9977	0.9718	1.4431	1.4099	0.7938	0.7807	5.8608	5.8098	24.44	25.13
Aus	1.1762	1.0856	-5.1311	-4.9494	0.9444	0.9383	3.3762	4.7825	15.06	21.37
IN08	0.9814	0.8898	7.6181	8.8395	0.9242	0.9202	16.9455	15.4355	20.73	16.58
IN10	0.9964	0.9036	2.3174	2.6071	0.8831	0.8776	10.1314	9.7808	20.56	21.19
All	1.0535	0.9662	0.3086	0.7474	0.9292	0.9232	13.0704	12.3310	21.25	22.38

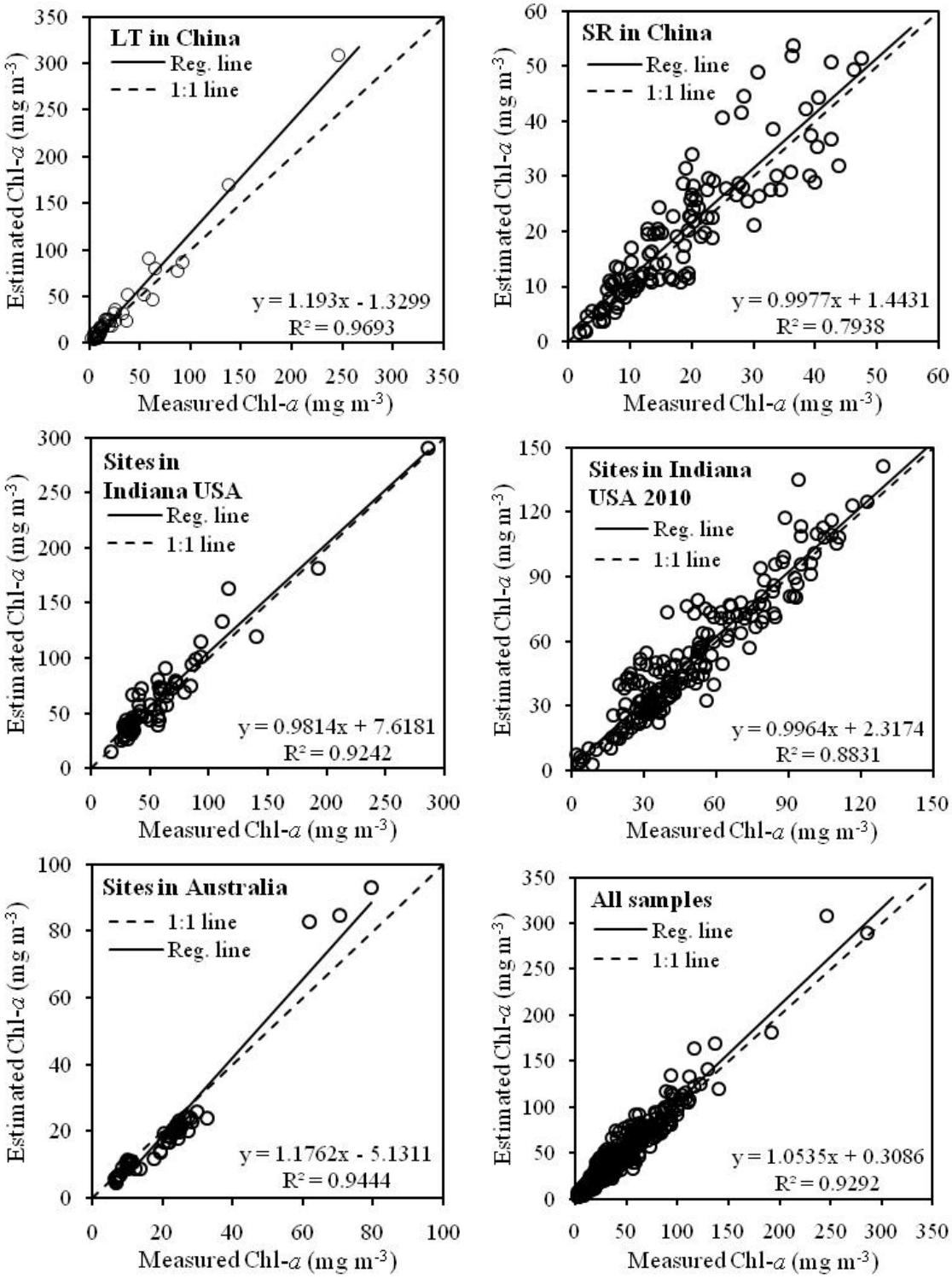

Fig. 2.7. Comparison between measured Chl-*a* and estimated Chl-*a* by equation 18.

The performances between equations 18 and 19 for the estimation of Chl-*a* concentration are compared by examining R^2, RMSE and MRE and shown in table 2.4.

Equation 19 is a simpler model than equation 18, and based on table 2.4 one can conclude that the performance of equation 19 almost matches that of equation 18 that requires the absorption coefficient at bands 630, 647, 665 and 691 nm. An interesting question is which model should be used when the absorption coefficient for phytoplankton or the bulk absorption for non-water constituents is available. The authors recommend that equation 19 should be preferred over equation 18 if $a^*_{ph}(665)$ is available and relatively constant because the former is simpler than the latter. In this paper, $a^*_{ph}(665)$ is set to be 0.016 m^2 (mg Chl-*a*)$^{-1}$ based on Gons et al. (2008), and then one may be curious how $a^*_{ph}(665)$ varies. To investigate the variability of $a^*_{ph}(665)$, $a^*_{ph}(665)$ for the water bodies investigated in this study was calculated by dividing the GTM-estimated $a_{ph}(665)$ ($\approx a_{t\text{-}w}(665)$) by measured Chl-*a* concentration with the assumption that $a_{t\text{-}w}(665)$ is accurately and exactly retrieved for all sites. The average values of estimated $a^*_{ph}(665)$ for different sites are shown in table 2.5. Variations of $a^*_{ph}(665)$ observed across the diferent water bodies are observed with the samples collected in Indiana 2008 have the highest $a^*_{ph}(665)$ (=0.0172 m^2 (mg Chl-*a*)$^{-1}$), the samples collected in Australia have the lowest $a^*_{ph}(665)$ (=0.0146 m^2 (mg Chl-*a*)$^{-1}$) and the averaged $a^*_{ph}(665)$ of all 477 samples equals to 0.0161 m^2 (mg Chl-*a*)$^{-1}$. This indicates that, while $a^*_{ph}(665)$ should be slightly different, $a^*_{ph}(665)$=0.016 m^2 (mg Chl-*a*)$^{-1}$ is appropriate for all inland waters investigated, and may be appropriate for inland water monitoring at the global scale. In fact, Bricaud et al. (1995) and Allali et al. (1997) asserted that $a^*_{ph}(\lambda)$ around 675 nm should be relatively stable without many impacts of accessory pigments. The use of

$a^*_{ph}(665)$ =0.016 m^2 and equation 19 provides an alternative to equation 18 for estimating Chl-*a* from the derived absorption coefficient with GTM. Such approach could be applied to some multi-spectral images acquired by the sensor MODIS, which do not have the four bands required by equation 18.

Table 2.5. GTM-Estimated $a^*_{ph}(665)$ for the investigated sites and that by Gons et al. (2008). $a^*_{ph}(665)$ are estimated by dividing estimated $a_{t\text{-}w}(665)$ with measured Chl-*a*.

Study site	LT	SR	Aus	IN08	IN10	All	Gons
Averaged $a^*_{ph}(665)$ m^2 (mg Chl-*a*)$^{-1}$	0.0171	0.0169	0.0146	0.0172	0.0159	0.0161	0.0160

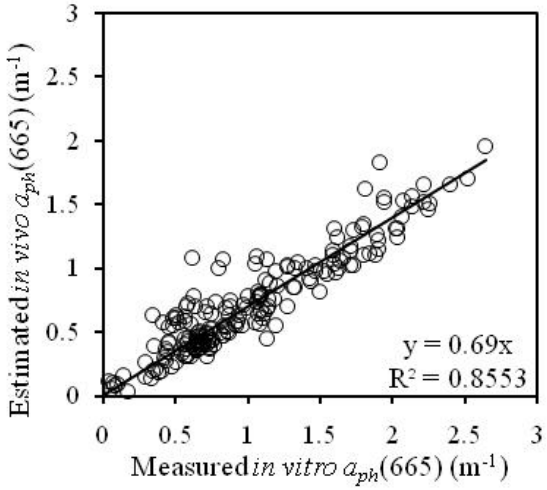

Fig. 2.8. Estimated *in vivo* $a_{ph}(665)$ (=$a_{t\text{-}w}(665)$) vs. measured *in vitro* $a_{ph}(665)$ (also $a_{sol}(665)$). *In vitro* peak at 665 nm is corresponding to *in vivo* peak 675 nm due to the band shift effect. This figure shows the conversion between *in vivo* $a_{ph}(665)$ and *in vitro* $a_{ph}(665)$.

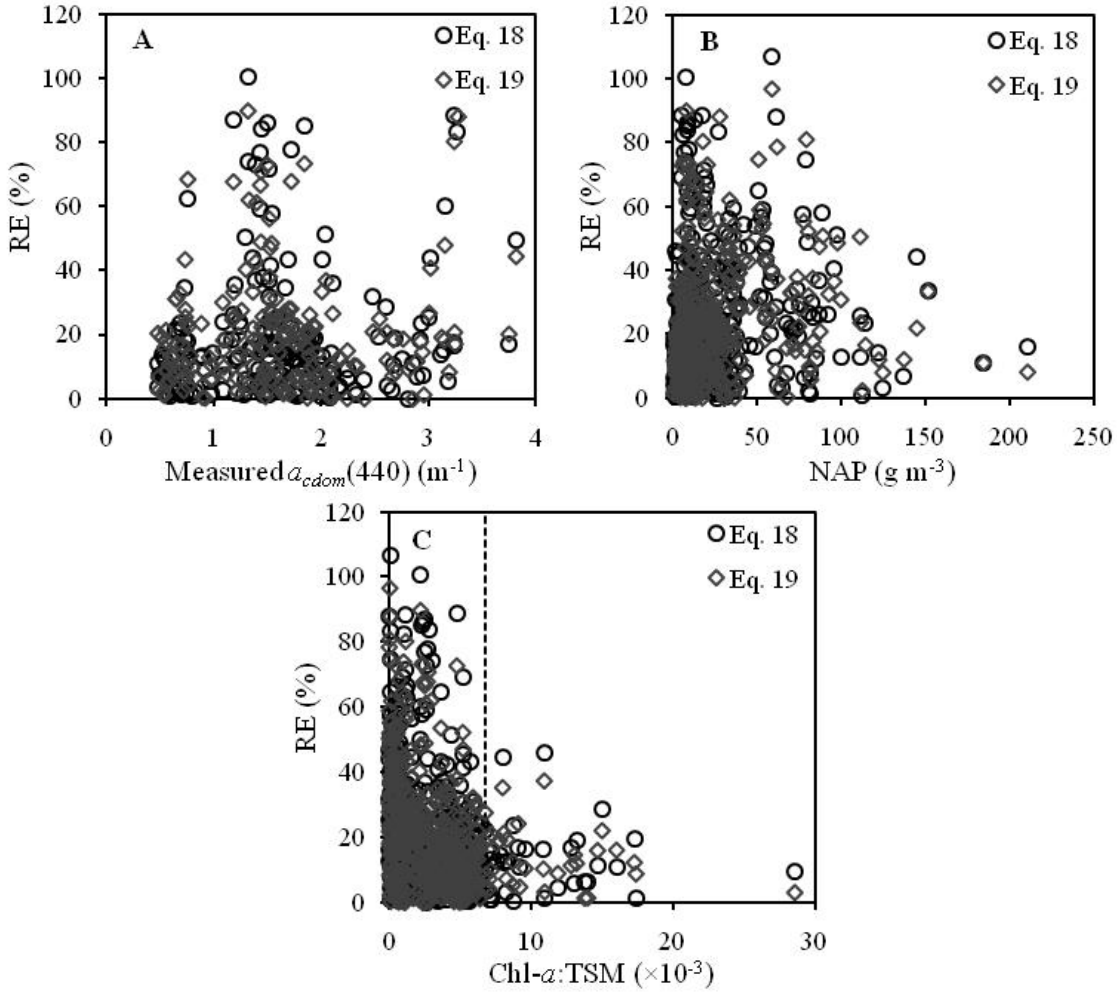

Fig. 2.9. Comparison between relative error (RE, equation 21) and possible interfering factor for estimating Chl-*a*. Each figure shows the RE resulted from estimation by equation 18 and equation 19, respectively. A: RE vs. $a_{cdom}(440)$; B: RE vs. NAP; C: Relative error vs. Chl-*a*/TSM.

Does this mean that equation 18 has no advantages over equation 19? Equation 18 achieves Chl-*a* estimation without the requirment for $a^*_{ph}(665)$ but for the absorption coefficients at the four bands. In addition to equation 18, Ritchie (2008) also proposed another four equations to estimate chlorophyll-*b* (Chl-*b*), -*c* (Chl-*c*), -*d* (Chl-*d*) and total chlorophylls from measured $a_{sol}(\lambda)$, respectively, and these equations use the same four

bands used in equation 18. Estimating accessory pigments, like Chl-*b*, -*c* and –*d* facilitates the identification of different phytoplankton species because accessory pigments contained in different species are not identical (Richardson, 1996). The information of phytoplankton species structure can help understand the impact of global climate change on phytoplankton community composition and the seasonal and regional variability of bio-optical properties in water bodies (Mao et al., 2010). Therefore we recommend that equation 18 should be used for estimating Chl-*a* from the derived absorption coefficients together with another four equations for Chl-*b*, -*c*, -*d* and total chlorophylls when these accessary pigments are of importance in remote water quality monitoring.

5.3.2 Factors interfering with Chl-a retrieval

The factors that could affect the GTM performance and in turn Chl-*a* estimation include the presence of algal scums, CDOM and NAP. Aglal scums could fail the GTM algorithm because they show obvious vegetation spectral features in the near-infared region. GTM uses $r_{rs}(778)$ to estimate $b_b(778)$ (equation 11). When algal scum happens, $r_{rs}(778)$ becomes higher than 0.082, leading to negative backscattering coefficients and failure of estimating $a_{t\text{-}w}(\lambda)$. As a result, Chl-*a* cannot be predicted from the erroneously estimated $a_{t\text{-}w}(\lambda)$. In this study, seventeen remote sensing reflectance spectra measured in LT were excluded. It is suggested to use the floating algal index (FAI, a simple MODIS spectral algebra; Hu, 2009) to detect algal scums before estimating Chl-*a* with the GTM algorithm. In this study, the longest wavelength for the measured reflectance spectra is 1075 nm and not all bands are available for calculating FAI. The spectra for the 17 sample stations were removed from the datasets manually.

For the case where algal scums are absent, high concentration of CDOM and NAP are major interfering factors for estimation of Chl-*a* in inland waters (Bukata, 1995; Schalles et al., 2001; Schalles, 2006; Zhou et al., 2009). To evaluate this effect, the relationship between $a_{cdom}(440)$ used for the proxy of CDOM concentration and RE (equation 21) for samples collected in Indiana 2010 is shown in Fig. 2.9.A. Fig. 2.9.A shows that the correlation between RE and $a_{cdom}(440)$ is not significant, implying that CDOM does not affect the Chl-*a* estimation. In fact, CDOM primarily absorbs at the wavelengths shorter than 620 nm and its absorption descreases exponentially with the increased wavelength. The CDOM absorption has no impacts on the GTM performance in estimating Chl-*a* from the derived $a_{t\text{-}w}(\lambda)$ because the GTM derivation is involved with the red and near-infrared region. NAP has a similar absorption spectra shape to CDOM, but results in strong scattering. As a result, NAP might have some impacts on Chl-*a* estimation. The NAP concentration was calculated according to the relationship shown in equation 23 (Hoogenboom et al., 1998; Sun et al., 2010).

$$\mathrm{NAP}(\mathrm{g\,m^{-3}}) = \mathrm{TSM}(\mathrm{g\,m^{-3}}) - 0.07\,\mathrm{Chl}-a(\mathrm{mg\,m^{-3}}) \tag{23}$$

The correlation between RE and NAP for all samples is shown in Fig. 2.9.B, and the triangle like pattern indicates that NAP do have some impacts on Chl-*a* estimation. Briefly, many samples with Chl-*a*:TSM less than 6.7942×10^{-3} (indicated by vertical dash line in Fig. 2.9.C) that is equivalent to the contribution of NAP to TSM more than 52.44% have an RE larger than 30%. This is attributed to the masking effect of NAP on the spectral signal of phytoplankton (Zhou et al., 2009). For the NAP-dominant other than phytoplankton-dominant water body, the GTM performance for estimating Chl-*a* needs improvment.

5.4 Application on simulated MERIS spectra

To test the applicability of GTM to MERIS image spectra, simulated datasets were generated by resampling field measured hyperspectral reflectance spectra to MERIS spectral reolution with ENVI 4.5 (ITT, Inc., Boulder, CO, USA) (Fig. 2.10. A). The simulated MERIS band 2 (443 nm), band 5 (560 nm), band 9 (708 nm) and band 12 (778 nm) were input to GTM for deriving the absorption and backscattering coefficients. Fig. 2.10.B shows the retrieved $a_{t\text{-}w}(\lambda)$ from simulated MERIS image spectra for the same samples shown in Fig. 2.4.A. However, equation 18 cannot be used to estimate Chl-*a* directly from predicted $a_{t\text{-}w}(\lambda)$ because the required bands at 630 nm, 647 nm and 691 nm are not available. Alternatively, using the available bands 620 nm (band 6), 665 nm (band 7) and 681 nm (band 8), a model (equation 24) is established using the same method in Ritchie (2008) based on $a_{sol}(\lambda)$ shown in Fig. 2.3.

$$\text{Chl}-a(\text{mg m}^{-3})=[-0.4371a_{ph}(620)+12.0186a_{ph}(665)/0.68-2.8558a_{ph}(681)]\times 4.34 \quad (24)$$

Equation 24 is valuable when $a^{*}_{ph}(665)$ is unknown; otherwise equation 19 should be used. In this study, the results by both equations 24 and 19 are shown in Fig. 2.10.C and Fig. 2.10.D, respectively. Both equations perform well for samples collected from all sites with R^2=0.906 (eq. 24) and R^2=0.9138 (eq. 19), respectively. Compared with the results derived from hyperspectral remote sensing spectra, the resultant R^2 and MRE from the simulated datasets have a slight degradation. Nonetheless, as indicated by the decent R^2 and MRE values, GTM can be used to estimate Chl-*a* from MERIS spectra.

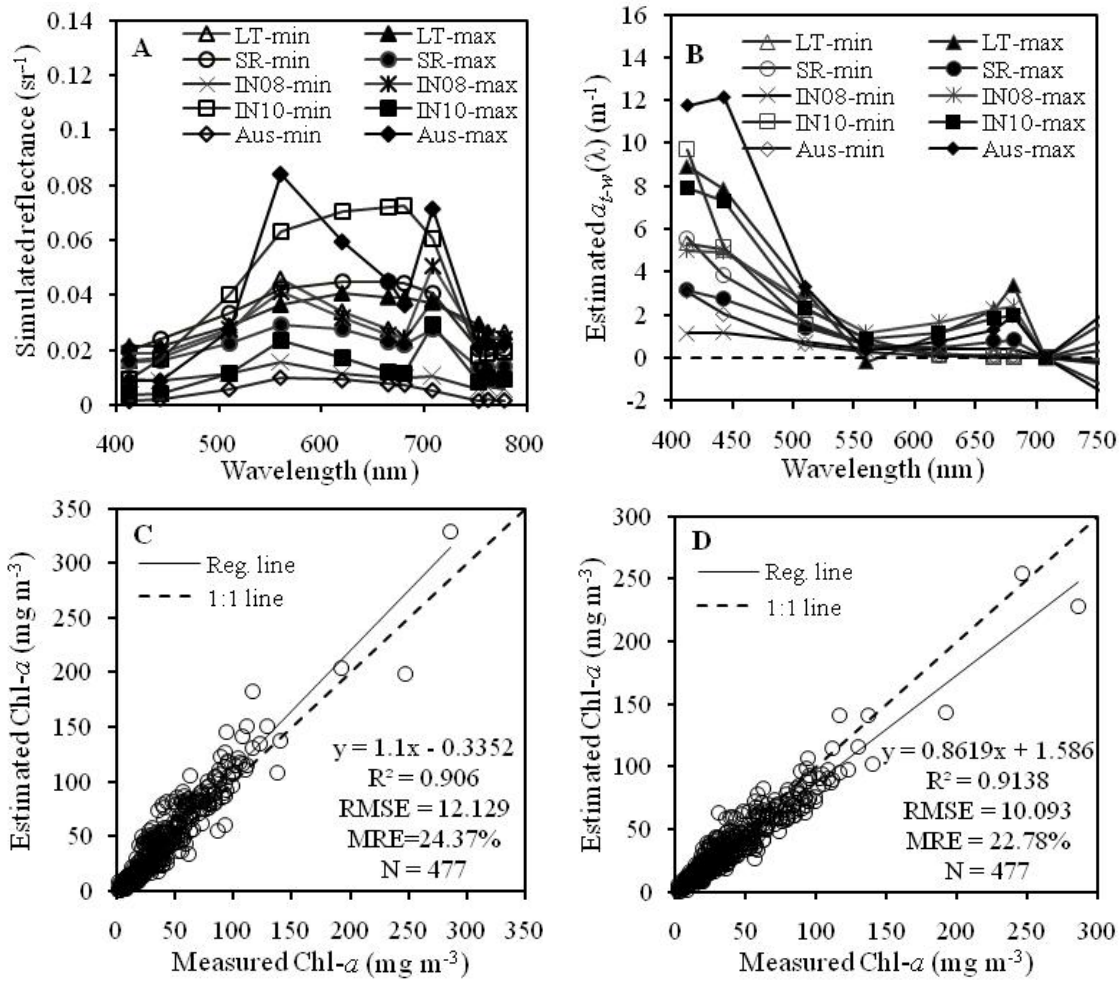

Fig. 2.10. A: Simulated MERIS imagery spectra; B: GTM-estimated $a_{t\text{-}w}(\lambda)$ based on A; C: estimated Chl-*a* vs. measured Chl-*a* using equation 24; D: estimated Chl-*a* vs. measured Chl-*a* using equation 19.

6. Conclusions

GTM was proposed and tested on field measured hyperspectral remote sensing reflectance in eight different reservoirs, lakes, and estuaries and in different seasons. It proves that the absorption coefficients could be more accurately retrieved when using a dynamic $\frac{f}{Q}$ (or g_1) for the model of equation 2. GTM retrieves $a_{t\text{-}w}(\lambda)$ spectra in water bodies dominated by either phytoplankton or CDM or water bodies with no dominant

constituent at all. The predicted $a_{t\text{-}w}(443)$ and $a_{t\text{-}w}(675)$ fit very well with measured ones, while $a_{t\text{-}w}(560)$ is dramatically underestimated, which might be due to ignoring the quadratic term in equation 1. However, based on accurately estimated $a_{t\text{-}w}(\lambda)$ at 630, 647, 665 and 691 nm, Chl-*a* was calculated using laboratory-derived equation (equation 18; Ritchie, 2008) and good accuracy was achieved for all study sites, when the accuracy is comparable using only $a_{t\text{-}w}(665)$ by equation 19. In fact, the good results by equation 19 evidently support that $a^*_{ph}(665)$ is stable in global scale although small variation exists.

The application of GTM on simulated MERIS spectra was also made to examine the potentials of the model for satellite surveillance of bio-optical properties in inland waters. The $a_{t\text{-}w}(\lambda)$ was predicted from simulated MERIS spectra using GTM without any modification, and subsequently, Chl-*a* was accurately retrieved by two approaches as well. Although the performance of the models somewhat degrades due to reduced spectral resolution compared to field measured remote sensing reflectance spectra, it exhibits great potentials for future satellite monitoring of inland waters with MERIS imagery. This will significantly drives our understanding on bio-optical status of inland waters.

Acknowledgements

The authors like to thank Center of Earth and Environmental Sciences (CEES), Shuai Li, Dawei Liu and Ying Sun from Indiana University-Purdue University at Indianapolis (IUPUI) for assisting field water sampling in the Indiana sites. The authors appreciate the financial support from the NASA Energy and Water Cycle Study program (Grant No. NNX09AU87G) and Key Knowledge Innovation Projects of the Chinese Academy of Sciences (KZCX2-YW-QN-305).

III. A GLOBALLY TRANSFERABLE MODEL FOR INLAND WATERS (II): PARTITIONING NON-WATER ABSORPTION COEFFICIENTS AND ESTIMATING PHYCOCYANIN [*]

ABSTRACT

Phycocynin (PC) primarily exists in toxic freshwater cyanobacteria. Accurate estimation of low PC concentration is critical to early warn potential risks of cyanobacterial population growth to the public. By the aid of absorption coefficients of acetone-extracted pigments, phytoplankton and colored detritus matter absorption were successfully predicted from a globally transferable model (GTM) estimated non-water absorption coefficients with R^2>0.785 and R^2=0.844, respectively. Meanwhile, PC absorption at 620 nm was derived, and thus PC concentrations were retrieved with relative root mean square error as 30.6% (R^2=0.798, *n*=151) with a fixed PC specific absorption coefficient from literature, and thus no calibration was made. No significant overestimation was observed for samples of low PC concentration, which is commonly the case of semi-empirical algorithm. The improvement is evidently due to the elimination of colored detritus matter absorption and consideration of pigment composition. Therefore, the method is suggested to be suitable for detection of PC in inland waters and it is not necessary that cyanobacteria are the dominant phytoplankton species, albeit stochastically high uncertainties happen for several low PC concentration samples. Particularly, accurate estimation based on simulated Medium Resolution Imaging Spectrometer reflectance spectra implies it becomes feasible for routine surveillance of cyanobacterial biomass dynamics in the future.

[*] The manuscript was submitted to Remote Sensing of Environments for review.

Keywords: globally transferable model, phycocyanin, absorption partitioning, cyanobacteria, MERIS

1. Introduction

Cyanobacteria, the largest and most diverse group of prokaryotes, can multiply very quickly in the warm summer when temperature, light and nutrient runoff from agriculture fertilizer increase (Mishra et al., 2009). Cyanobacteria are usually the dominant phytoplankton species in eutrophic lakes, estuaries, and reservoirs, due to several key adaptations: buoyancy regulation, nitrogen fixing capability, and harvesting yellow-orange light for photosynthesis (Jupp et al., 1994; Paerl & Huisman, 2009). When cyanobacterial blooms happen in drinking and recreational waters, recreational activities and aquatic habitats are hampered, the aesthetics of the water is destroyed and human and animals' health is threatened (Codd et al., 1999; Kuster et al., 2006; Mishra et al., 2009; Randolph et al., 2008). Therefore, cyanobacterial blooms are one of the most important issues faced by environmental agencies, water authorities and public health organizations (Backer, 2002).

Cyanobacterial biomass can be assessed by detecting and quantifying phycocyanin (PC), an accessory pigment that is primarily present in freshwater cyanobacteria and plays significant role in cyanobacterial light harvesting. The presence of cyanobacteria in fresh water generally results in remote sensing reflectance depression around 620-630 nm caused by PC absorption (Metsamaa et al., 2006). Based on this spectrally diagnostic absorption, many efforts on remote quantification of cyanobacterial pigments have been made and focused on the empirical approach to deriving PC from reflectance band ratio

(Hunter et al., 2008 & 2009; Li et al., 2010; Mishra et al., 2009; Schalles & Yacobi, 2000; Ruiz-Verdu et al., 2008), band combinations (Dekker, 1993; Hunter et al., 2010; Li et al., 2010; Vincent et al., 2004), and on semi-empirical algorithms (Simis et al., 2005 & 2007) using PC absorption (Guanter et al., 2010; Hunter et al., 2010; Randolph et al., 2008; Ruiz-Verdu et al., 2008; Yang & Pan, 2006;). Empirical algorithms are limited to the dataset where they are derived (Giardino et al., 2007; Matthews et al., 2010), while the semi-empirical algorithm usually predicts PC without recalibration. The semi-empirical algorithm derives PC bulk absorption at 620 nm, and then takes the ratio of the PC bulk absorption to specific absorption to calculate PC concentration (see section 2.5 for model description). However, the semi-empirical algorithm does not perform as well at low PC concentration (PC<50 mg m^{-3}) as at high PC concentration (Simis et al. 2007). In fact, an intercept of 29 mg PC m^{-3} is present in the correlation between measured and estimated PC in Simis et al. (2005) implying overestimated PC. Two reasons may be responsible for its degraded performance at low PC concentration: 1) failing to remove the absorption of colored dissolved organic matter (CDOM) and non-algal particles (NAP) (hereafter CDOM+NAP will be referred as CDM) when deriving $a_{pc}(620)$ and 2) inaccurate estimation of the PC absorption ($a_{pc}(\lambda)$; *refer to table 3.1 for symbols*) at 620 nm from phytoplankton absorption ($a_{ph}(\lambda)$) using the relationship $a_{pc}(620)=a_{ph}(620)-0.24a_{ph}(665)$. In fact, CDM absorption ($a_{cdm}(\lambda)$) could induce a significant error in estimated $a_{pc}(620)$. For example, based on the relationship $a_{cdm}(\lambda)=a_{cdm}(\lambda_0)\exp[-S_{cdm}(\lambda-\lambda_0)]$ (S_{cdm} is exponential slope of CDM absorption; Ciotti and Bricaud 2006; Oubelkheir et al. 2007) and setting λ_0=443 nm, $a_{cdm}(443)$=1.5 m^{-1} and S_{cdm}=0.015 nm^{-1} for turbid waters, one can estimate $a_{cdm}(620)$ to be 0.1055 m^{-1}, which is equivalent to overestimated PC

concentration 24.53 mg PC m^{-3} if $a^*_{pc}(620)$ =0.0043 m^2 (mg PC)$^{-1}$ is assumed (Jupp et al., 1994). In addition, the fraction constant 0.24, used in $a_{pc}(620)=a_{ph}(620)-0.24a_{ph}(665)$ to correct the proportion of chlorophyll-a (Chl-*a*) and accessory pigments absorption at 620 nm, is not valid when pigments composition changes (Simis et al., 2007), resulting in increased uncertainties in estimated PC concentration when PC:Chl-*a* is less than 0.5 (Hunter et al. 2010).

These weaknesses of the semi-empirical algorithm imply that to improve PC estimation the absorption of CDM and other pigments has to be isolated. Non-water absorption coefficients ($a_{t\text{-}w}(\lambda)$; $a_{t\text{-}w}(\lambda)=a_{ph}(\lambda)+a_{cdm}(\lambda)$) can be accurately retrieved using the GTM algorithm for eutrophic and turbid inland waters (Chapter 2). If $a_{t\text{-}w}(\lambda)$ could be partitioned into $a_{cdm}(\lambda)$, $a_{pc}(\lambda)$ and absorption of other pigments ($a_{ph\text{-}pc}(\lambda)$; $a_{ph\text{-}pc}(\lambda)=a_{ph}(\lambda)-a_{pc}(\lambda)$), then $a_{pc}(620)$ could be predicted from which the impacts of CDM and other pigments are removed. While several methods (Ciotti & Bricaud 2006; Oubelkheir et al. 2007; Wang et al. 2009; Zhang et al. 2009) are available for separating $a_{ph}(\lambda)$ and non-phytoplankton absorption (either $a_{cdm}(\lambda)$ or $a_{nap}(\lambda)$), they fail to retrieve $a_{pc}(620)$ because $a_{pc}(\lambda)$ is not considered as an independent component in the retrieval. As a result, a new approach to the absorption retrieval where PC is treated as an independent component is required.

In this study, a new approach is proposed for deriving $a_{pc}(620)$, in which the phytoplankton and CDM absorption are partitioned from a globally transferable model (GTM)-estimated non-water absorption coefficients. The aim is 1) to develop a new algorithm to partition non-water absorption coefficients with $a_{pc}(620)$ as an independent component; 2) to examine whether the new algorithm could improve the accuracy of

retrieval of PC, especially for samples with low PC. If the algorithm can be used for retrieval of low PC, it will permit early warning of cyanobacterial blooms with remote sensing data (Hunter et al. 2009).

Table 3.1. List of symbols and acronyms.

Symbol/ acronym	Description	Units
$b_b(\lambda)$	Total backscattering coefficients at wavelength λ.	m^{-1}
$b_{bp}(\lambda)$	Backscattering coefficients of particles at wavelength λ.	m^{-1}
$a^*_{pc}(\lambda)$	PC specific absorption coefficients at wavelength λ.	m^2 (mg PC)$^{-1}$
$a_i(\lambda)$	Absorption coefficients of compound *i* at wavelength λ. Subscripts used: *t-w* = non-water; *ph* = phytoplankton; *cdm* = colored detritus matter; *pc* = phycocyanin; *sol* = extracted phytoplankton pigments; *ph-pc*: phytoplankton pigments excluding phycocyanin; *cdm+pc*: colored detritus matter plus phycocyanin.	m^{-1}
S_{cdm}	Exponential slope of $a_{cdm}(\lambda)$; $a_{cdm}(\lambda)= a_{cdm}(\lambda_0)\exp[-S_{cdm}\times(\lambda-\lambda_0)]$	nm^{-1}
$R_{rs}(\lambda)$	Above water surface remote sensing reflectance at wavelength λ.	sr^{-1}
$r_{rs}(\lambda)$	Below water surface remote sensing reflectance at wavelength λ.	sr^{-1}
PC	Phycocyanin (concentration)	mg m^{-3}
Chl-*a*	Chlorophyll-a (concentration)	mg m^{-3}
PE	Phycoerythrin	-
CDM	Colored detritus matter	-
rRMSE	Relative root mean square error	-
RE	Relative error	-

2. Materials and Methods

2.1. Study sites

The study sites are three central Indiana reservoirs: Eagle Creek Reservoir (ECR) (39°51' N, 86°18.3' W), Geist Reservoir (GR) (39°55' N, 85°56.7' W) and Morse Reservoir (MR) (40°6.4' N, 86°2.3' W). These reservoirs have similar depth (3.2-4.7 m), surface area (5-7.5 km^2), volume (21-28 million m^3) and residence time (55-70 days). They were selected for the study because of their importance for supplying drinking

water to residents surrounding the Indianapolis metropolitan area, and they all face a serious eutrophication problem- toxic cyanobacterial blooms. Ten field campaigns were conducted on these three reservoirs in 2010 and the statistical information of the measurements for these campaigns is listed in table 3.2.

Table 3.2. Statistical information of pigments concentrations and PC:Chl-*a* ratio.

Site	Date	Chl-*a* (mg m^{-3})				PC (mg m^{-3})				PC:Chl-*a*		
		n	min	max	avg.	*n*	min	max	avg.	min	max	avg.
ECR	May-Oct 2010	80	21.62	128.04	54.51	60	8.58	69.66	29.23	0.17	2.05	0.66
MR	Jun-Oct 2010	56	8.31	62.12	34.47	54	1.46	146.10	90.47	0.49	1.86	1.72
GR	Apr-Oct 2010	54	1.85	129.39	60.21	37	6.57	140.76	64.90	0.14	3.45	1.76

2.2. Reflectance measurement

An Ocean Optics USB4000 (Ocean Optics, Inc., Dunedin, FL, USA) unit with dual radiometers was used to measure below surface remote sensing reflectance ($r_{rs}(\lambda)$) in the three central Indiana reservoirs in 2010. Reflectance measurement was made by following the procedure described by Gitelson et al. (2008). Mounted on a 2 m high pole, radiometer 1 was pointed upward to measure the real-time incidence $E_d(0+,\lambda)$, and simultaneously radiometer 2, equipped with a 25° field-of-view optical fiber, was dipped ~2 cm below the water surface with a 2 m-long pole to measure the below-surface upwelling radiance $L_u(0-,\lambda)$ on the sunny side at nadir. *In situ* spectra were then processed in laboratory using the software CALMIT Data Acquisition Program (CDAP, University of Nebraska at Lincoln) to compute $r_{rs}'(\lambda)$:

$$r_{rs}'(\lambda)=\frac{L_u(0-,\lambda)}{E_d(0+,\lambda)} \quad (1)$$

Based on the relationship $E_d(0-,\lambda)=0.965E_d(0+,\lambda)$ (Morel and Maritorena (2001), remote sensing reflectance below the water surface ($r_{rs}(\lambda)$) can be computed as below:

$$r_{rs}(\lambda)=\frac{r_{rs}'(\lambda)}{0.965} \quad (2)$$

The computed remote sensing reflectance spectra below the water surface are shown in Fig. 3.1.

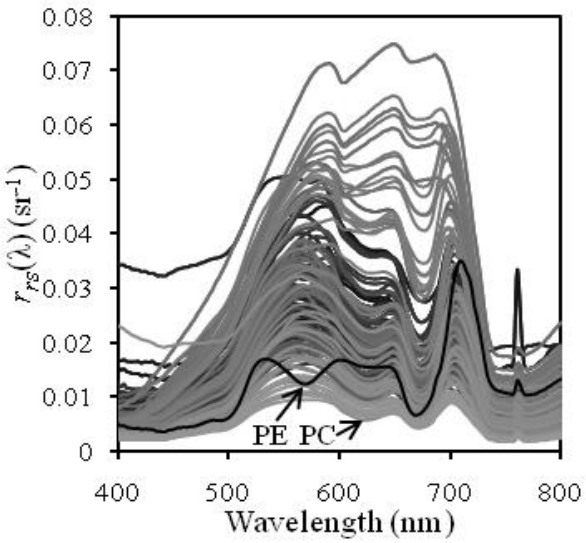

Fig. 3.1. Measured below surface remote sensing reflectance $r_{rs}(\lambda)$. PE: depression due to phycoerythrin (PE) absorption; PC: depression due to PC absorption.

2.3. Pigments extraction and quantification

Water samples were collected using 1 L amber HDPE bottle at all sites where *in situ* reflectance was measured, and then temporarily stored in cold and dark coolers. Once back to laboratory, samples were filtered and frozen immediately to prevent pigments denaturalization. Water samples for Chl-*a* extraction passed 0.45 μm pore size acetate filters (Whatman), after which Chl-*a* was extracted with 90% acetone for about 24 hours. The optical density of Chl-*a* extracts in solution ($OD_{sol}(\lambda)$) was measured using a spectrophotometer with the spectral range of 380-750 nm at 1 nm resolution, and Chl-*a* concentration was then determined by applying the equation given in Ritchie (2008) to

the measured $OD_{sol}(\lambda)$. The absorption of Chl-*a* extracts in solution ($a_{sol}(\lambda)$, also referred as *in vitro* $a_{ph}(\lambda)$) was also derived from the $OD_{sol}(\lambda)$ according to Beer's Law.

$$a_{sol}(\lambda)=2.303OD_{sol}(\lambda)/l \quad (3)$$

where 2.303 is used to convert the 10-base log to natural log and l (=0.01 m) is the optical path length.

For the determination of PC concentration, a homogenization method with a tissue grinder was modified to improve the accuracy of measurements (Sarada et al., 1999; Randolph et al. 2008). Samples were filtered through 0.7 μm pore size glass fiber filter (Millipore APFF). The filters were then transferred to 50 milliliter polycarbonate centrifuge tube and broken up in 50 mmol L^{-1} sodium phosphate buffer (pH 7.0$\pm$0.2) using a stainless steel spatula. The broken filters then went through the first round of grinding and centrifuge. After being stored in freezer (4 ^{o}C) for 24 hours, filters were grinded and centrifuged again with the same equipments. PC concentration of upper supernatant was fluorometrically determined using TD700-fluorometer (Turner Designs, Inc.). The fluorometer was pre-calibrated with PC solutions produced with highly purified, lyophilized PC powder (Sigma-Aldrich P6161).

2.4. Absorption coefficient in laboratory

The measured $a_{sol}(\lambda)$ above is *in vitro* phytoplankton absorption without PC contribution because PC is not soluble in acetone buffer, which can be used to derive *in vivo* phytoplankton absorption without PC contribution ($a_{ph\text{-}pc}(\lambda)$). Our rationale is that both *in vivo* phytoplankton absorption $a_{ph}(\lambda)$ with PC contribution and $a_{ph\text{-}pc}(\lambda)$ can be estimated from remote sensing reflectance. However, several studies have shown that band shifts exist between *in vivo* and *in vitro* $a_{ph}(\lambda)$ (Emerson & Lewis 1942; Shibata et

al. 1954; Myers & Kratz 1955). To be compatible with *in vivo* $a_{ph}(\lambda)$, the correction for this band shift on $a_{sol}(\lambda)$ is required and was completed by manually adjusting $a_{sol}(\lambda)$ toward longer wavelength according to Emerson and Lewis (1942). Briefly, the $a_{sol}(\lambda)$ spectra were divided into three groups, $a_{sol}(\lambda)$ at $\lambda<480$ nm was shifted by 8 nm, 480 nm$\leq \lambda \leq$580 nm by 13 nm, $\lambda>580$ nm by 10 nm, and finally the 5 nm gap between 488 nm and 493 nm was interpolated using the spline approach and the overlapping of 591-593 nm is set to the original values at 578-580 nm because, before shifting, $a_{sol}(\lambda)$ at 578-583 nm is relatively flat. As a result, the adjusted $a_{sol}(\lambda)$ has the same wavelength alignment as the corresponding *in vivo* spectra, and is denoted by $a_{ph\text{-}pc}(\lambda)$ hereafter. The $a_{ph\text{-}pc}(\lambda)$ spectra are shown in Fig. 3.2.A.

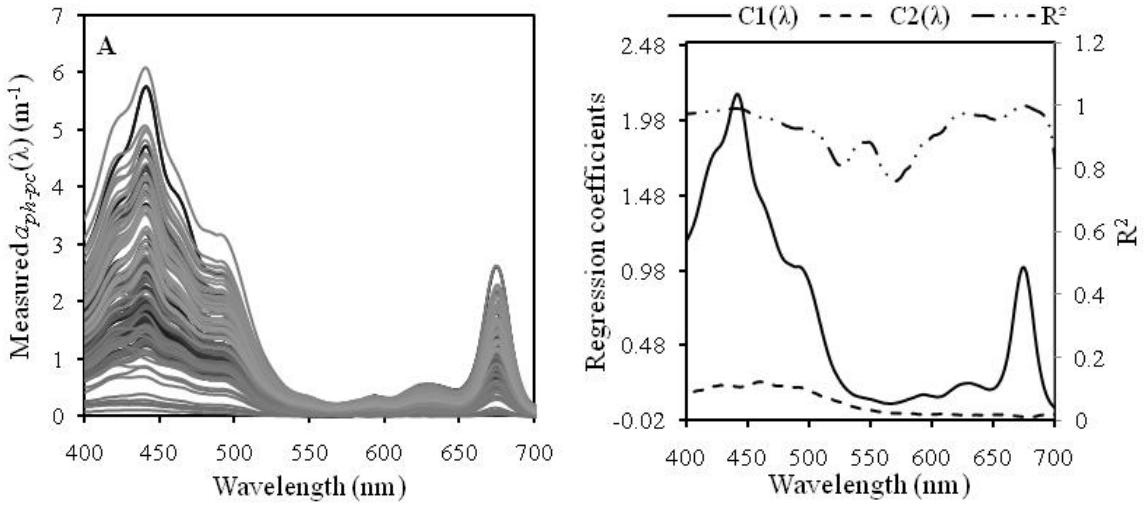

Fig. 3.2. A: *in vivo* $a_{ph\text{-}pc}(\lambda)$ by adjusting $a_{sol}(\lambda)$ measured in 90% acetone extraction; B: regression coefficients (left axis) and R^2 (right axis) for equation 4 using dataset in A.

Several previous studies (e.g. Sun et al., 2010; Wang et al., 2009 & 2010) suggested that *in vivo* $a_{ph}(\lambda)$ could be expressed as a function of absorption peak value at either 443 nm or 675 nm. Application of this rule to $a_{ph\text{-}pc}(\lambda)$ results in equation 4:

$$a_{ph-pc}(\lambda)=\mathrm{C1}(\lambda)a_{ph-pc}(675)+\mathrm{C2}(\lambda) \quad (4)$$

where C1(λ) and C2(λ) are the regression coefficients. The values for C1(λ) and C2(λ) are shown in Fig. 3.2.B.

To obtain *in vivo* $a_{ph}(\lambda)$ in laboratory, the absorption coefficient of non-water constituents ($a_{t\text{-}w}(\lambda)=a_{ph}(\lambda)+a_{cdm}(\lambda)$) was first measured. The unfiltered water samples were poured into 1-cm cuvette and scanned by a spectrophotometer (380-800 nm, 1 nm resolution) with Milli-Q water as the reference, and the optical density ($OD_{t\text{-}w}(\lambda)$) was then determined for each sample (forty samples were excluded due to inappropriate storage). Subsequently, $OD_{t\text{-}w}(750)$ was subtracted from $OD_{t\text{-}w}(\lambda)$ for correcting backscattering effect and then converted to $a_{t\text{-}w}(\lambda)$ with equation 5:

$$a_{t-w}(\lambda)=2.303OD_{t-w}(\lambda)/l \tag{5}$$

The absorption spectra were then smoothed using the spline function implemented in MATLAB (MathWorks, Inc., Natick, MA, USA).

$a_{t\text{-}w}(\lambda)$ is the sum of $a_{ph}(\lambda)$ and $a_{cdm}(\lambda)$, from which $a_{ph}(\lambda)$ and $a_{cdm}(\lambda)$ can be derived. Bricaud & Stramski (1990) showed the following relationships for $a_{ph}(\lambda)$ and $a_{cdm}(\lambda)$:

$$a_{ph}(505):a_{ph}(380)=0.99 \tag{6a}$$

$$a_{ph}(580):a_{ph}(693)=0.92 \tag{6b}$$

$$a_{cdm}(\lambda)=A\exp(-\lambda\times S_{cdm}) \tag{6c}$$

$$a_{ph}(\lambda)=a_{t-w}(\lambda)-a_{cdm}(\lambda) \tag{6d}$$

where A is a constant for a given $a_{t\text{-}w}(\lambda)$ spectrum. The relationships 6e-6f can be generated by arranging equations 6a-6d:

$$0.99A\exp(-380S_{cdm})-A\exp(-505S_{cdm})=0.99a_{t-w}(380)-a_{t-w}(505) \tag{6e}$$

$$A\exp(-580S_{cdm})-0.92A\exp(-693S_{cdm})=a_{t-w}(580)-0.92a_{t-w}(693) \tag{6f}$$

Solving for A and S_{cdm} in equations 6e-6f, and then $a_{cdm}(\lambda)$ and $a_{ph}(\lambda)$ can be computed by inserting A and S_{cdm} values back to equations 6c-6d. Derived $a_{t\text{-}w}(\lambda)$, $a_{cdm}(\lambda)$ and $a_{ph}(\lambda)$ are shown in Fig. 3.3 in which $a_{cdm}(750)$ is forced to zero.

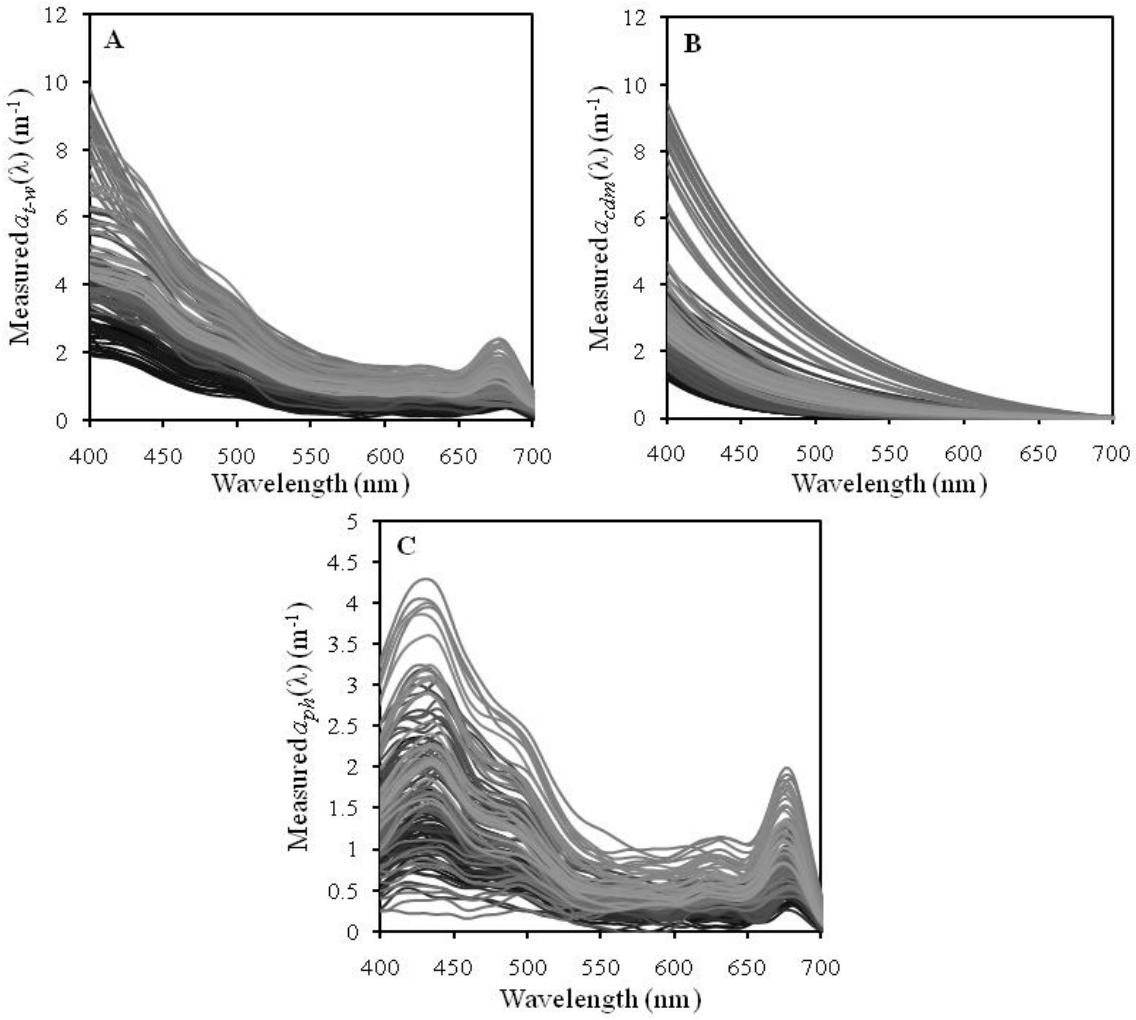

Fig. 3.3. A: measured $a_{t\text{-}w}(\lambda)$ from unfiltered water samples; B: measured $a_{cdm}(\lambda)$; C: measured $a_{ph}(\lambda)$. Forty samples are excluded due to inappropriate storage and total 151 samples are shown in this figure.

2.5. Remotely deriving absorption coefficients of phytoplankton, CDM and PC

The procedure for deriving $a_{ph}(\lambda)$, $a_{cdm}(\lambda)$ and $a_{pc}(\lambda)$ from remote sensing reflectance is built upon GTM which can remotely derive non-water constituents ($a_{t\text{-}w}(\lambda)$) and

estimate Chl-*a* concentration. GTM has been detailed in (Chapter 2) and therefore a brief description is given here. GTM starts with estimating backscattering coefficients ($b_b(\lambda)$) from remote sensing reflectance based on equation 7a (Gordon et al. 1988) by following the steps described in Gons et al. (2005) and Lee et al. (2002, 2004 & 2009), and $a_{t\text{-}w}(\lambda)$ is then retrieved by solving equation 7b constructed with reflectance band ratio.

$$r_{rs}(\lambda)=\frac{f}{Q}(\lambda)\frac{b_b(\lambda)}{a(\lambda)+b_b(\lambda)} \tag{7a}$$

$$\frac{r_{rs}(\lambda)}{r_{rs}(709)}=\frac{b_b(\lambda)[a_w(709)+b_b(709)]}{b_b(709)[a_w(\lambda)+a_{t-w}(\lambda)+b_b(\lambda)]} \tag{7b}$$

where f is the light field factor, Q stands for the light distribution factor defined as $Q=E_d(0)/L_u(0)$, and f/Q has only weak dependency on wavelength λ (Morel & Gentili, 1993 & 1996); $a_w(\lambda)$ represents water absorption coefficients given in Buiteveld et al. (1994); and the relationships for the total absorption coefficient $a(\lambda)=a_{t\text{-}w}(\lambda)+a_w(\lambda)$ and $a(709)\approx a_w(709)$ are used (Gons et al., 2008; Simis et al., 2005). The steps of GTM for deriving $a_{t\text{-}w}(\lambda)$ are shown in table 3.3 and the derived $a_{t\text{-}w}(\lambda)$ spectra are shown in Fig. 3.4. After derivation of $a_{t\text{-}w}(\lambda)$, an immediate task is to derive $a_{ph}(\lambda)$, $a_{cdm}(\lambda)$ and $a_{pc}(620)$ from $a_{t\text{-}w}(\lambda)$.

Many methods are available for partitioning $a_{t\text{-}w}(\lambda)$ into phytoplankton ($a_{ph}(\lambda)$) and colored detritus matter ($a_{cdm}(\lambda)$) absorptions, including those by Ciotti and Bricaud (2006; denoted as C06), Oubelkheir et al. (2007; denoted as O07) and Wang et al. (2009; denoted as W09). Both C06 and O07 are similar to the steps in equations 6a-6f but with different pairs of ratios from equations 6a and 6b, i.e. $a_{ph}(490):a_{ph}(412)=0.919\text{Chl-}a^{0.012}$ and $a_{ph}(510):a_{ph}(412)=0.581\text{Chl-}a^{0.047}$ for C06, and $a_{ph}(510):a_{ph}(412)=0.435$ and

$a_{ph}(555)$:$a_{ph}(630)$=0.98 for O07. W09 directly retrieves $a_{ph}(443)$, $a_{cdm}(443)$ and S_{cdm} by solving equations 8a-8c and then to derive $a_{cdm}(\lambda)$ and $a_{ph}(\lambda)$ by equation 8d-8e.

$$a_{t-w}(443)=a_{ph}(443)+a_{cdm}(443) \quad (8a)$$

$$a_{t-w}(412)=1.1365a_{ph}^{2}(443)+0.7171a_{ph}(443)+a_{cdm}(443)\exp[-S_{cdm}\times(412-443)] \quad (8b)$$

$$a_{t-w}(490)=2.7986a_{ph}^{2}(443)+0.6366a_{ph}(443)+a_{cdm}(443)\exp[-S_{cdm}\times(490-443)] \quad (8c)$$

$$a_{cdm}(\lambda)=a_{cdm}(443)\exp[-S_{cdm}\times(\lambda-443)]-a_{cdm}(443)\exp[-S_{cdm}\times(750-443)] \quad (8d)$$

$$a_{ph}(\lambda)=a_{t-w}(\lambda)-a_{cdm}(\lambda) \quad (8e)$$

However, the algorithm for isolating PC absorption from phytoplankton absorption are not available, a new method for this purpose is proposed in this study. The steps of this new algorithm are summarized in table 3.4. First, the algorithm uses the assumptions that $a_{cdm}(\lambda)$ for $\lambda\geq665$ nm is negligible and PC absorption is only limited in a narrow spectral range around 620 nm (Simis et al., 2005 & 2007), and this leads to $a_{ph\text{-}pc}(665)\approx a_{t\text{-}w}(665)$. Further analysis reveals that $a_{t\text{-}w}(665)$ and $a_{t\text{-}w}(675)$ are highly correlated (R^2=0.9739) and the relationship between them is shown in equation 9.

$$a_{ph-pc}(675)=a_{t-w}(675)=1.1872a_{t-w}(665) \quad (9)$$

Thereafter $a_{ph\text{-}pc}(\lambda)$ is predicted by substituting equation 9 in to equation 4, which is used to derive the absorption of CDM+PC ($a_{cdm+pc}(\lambda)$), i.e. the difference between $a_{t\text{-}w}(\lambda)$ and $a_{ph\text{-}pc}(\lambda)$.

$$a_{cdm+pc}(\lambda)=a_{t-w}(\lambda)-a_{ph-pc}(\lambda) \quad (10)$$

The next step is to derive $a_{cdm}(\lambda)$ based on equation 11a. Again based on the assumption that $a_{pc}(\lambda)$ is limited to narrow spectral range around 620 nm, $a_{cdm}(412)=a_{cdm+pc}(412)$ and $a_{cdm}(510)=a_{cdm+pc}(510)$ are assumed to be valid. The reason for choosing wavelengths 412

and 510 nm is that Medium Resolution Imaging Spectrometer (MERIS) is able to image at both the two wavelengths. Moreover band 443 nm was not recommended for retrieving $a_{cdm}(\lambda)$ due to the high variability of phytoplankton absorption at this wavelength (Hoge & Lyon, 1999; Hoge et al., 1999; references therein). Derivation of $a_{cdm}(\lambda)$ with $a_{cdm}(412)$ and $a_{cdm}(510)$ is shown in equation 11a-11b, and here 412 is set as reference wavelength. Subsequently, $a_{ph}(\lambda)$ is determined by equation 8e.

$$a_{cdm}(\lambda)=a_{cdm}(412)\exp[-S_{cdm}\times(\lambda-412)] \tag{11a}$$

$$S_{cdm}=-\frac{1}{98}\ln\frac{a_{cdm}(510)}{a_{cdm}(412)} \tag{11b}$$

Finally, $a_{pc}(\lambda)$ at the peak position 620 nm is calculated using equation 12. While PC absorption coefficient can be calculated for other wavelengths, they are too weak to be useful in PC concentration retrieval.

$$a_{pc}(620)=a_{cdm+pc}(620)-a_{cdm}(620) \tag{12}$$

In addition, $a_{pc}(620)$ can also be estimated using the semi-empirical algorithm developed by Simis et al. (2005 & 2007; equation 13a-13c).

$$b_b=b_b(778)=\frac{1.61\pi R_{rs}(778)}{0.082-0.6\pi R_{rs}(778)} \tag{13a}$$

$$a_{ph}(665)=1.47\times\left[\frac{R_{rs}(709)}{R_{rs}(665)}\times(0.727+b_b)-b_b-0.401\right] \tag{13b}$$

$$a_{pc}(620)=\left\{\left[\frac{R_{rs}(709)}{R_{rs}(620)}\times(0.727+b_b)-b_b-0.281\right]-0.24a_{ph}(665)\right\}\times 0.84^{-1} \tag{13c}$$

where $R_{rs}(\lambda)$ is the remote sensing reflectance above the water surface defined as $R_{rs}(\lambda)=L_w(0+,\lambda)/E_d(0+,\lambda)$ with $L_w(0+,\lambda)$ being the water-leaving radiance, and $R_{rs}(\lambda)=0.54r_{rs}(\lambda)$ (Gons et al., 2005).

Table 3.3. Globally transferable model (GTM) to derive IOPs and Chl-*a* concentration.

Step	Variable	Formula
1	$b_b(778)$	$b_b(778)=\frac{r_{rs}(778)a_w(778)}{0.082-r_{rs}(778)}$
2	Y	$Y=2.0\left[1-1.2\exp\left(-0.9\frac{r_{rs}(443)}{r_{rs}(560)}\right)\right]$ If necessary, $r_{rs}(\lambda)=\frac{R_{rs}(\lambda)}{0.52+1.7R_{rs}(\lambda)}$
3	$b_{bp}(560)$	$b_{bp}(560)=\frac{b_b(778)-b_{bw}(778)}{0.7198^{Y}}$
4	$b_b(\lambda)$	$b_b(\lambda)=b_{bp}(560)\left(\frac{560}{\lambda}\right)^{Y}+b_{bw}(\lambda)$
5	$a_{t-w}(\lambda)$	$a_{t-w}(\lambda)=\frac{R_x(709)b_b(\lambda)[a_w(709)+b_b(709)]}{R_x(\lambda)b_b(709)}-b_b(\lambda)-a_w($ where $R_x(\lambda)$ represents either $R_{rs}(\lambda)$ or $r_{rs}(\lambda)$
6	Chl-*a* (mg m^{-3})	$Chl-a=[-0.3319a_{sol}(630)-1.7485a_{sol}(647)+11.9442a_{sol}(665)-1.4306a_{sol}(691)]\times 4.34$ where $a_{sol}(665)=\frac{a_{t-w}(665)}{0.68}$ and $a_{sol}(\lambda_i)=a_{t-w}(\lambda_i)$ (λ_i=630, 647 and 691, respectively)
	Chl-*a* (mg m^{-3})	$Chl-a=\frac{a_{t-w}(665)}{a^*_{ph}(665)}$, $a^*_{ph}(665)=0.016$ m^2 (mg Chl-*a*)$^{-1}$

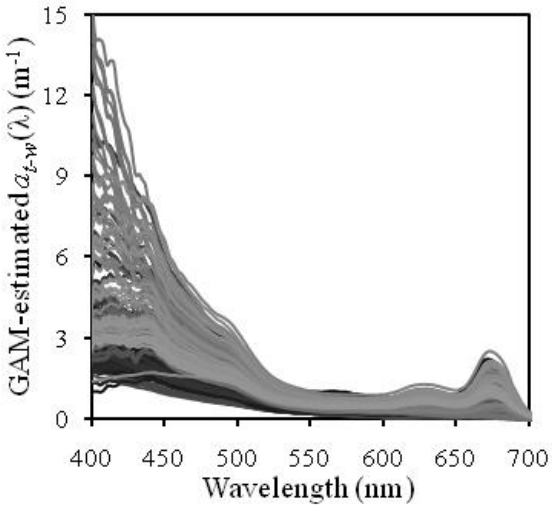

Fig. 3.4. Estimated $a_{t-w}(\lambda)$ using GTM for all samples collected in Indiana 2010.

Table 3.4. Extended steps of GTM to estimate $a_{cdm}(\lambda)$, $a_{ph}(\lambda)$ and PC.

Step	Variable	Formula
7	$a_{ph\text{-}pc}(\lambda)$	$a_{ph-pc}(\lambda)=1.1872C1(\lambda)a_{t-w}(665)+C2(\lambda)$
8	$a_{cdm+pc}(\lambda)$	$a_{cdm+pc}(\lambda)=a_{t-w}(\lambda)-a_{ph-pc}(\lambda)$
9	S_{cdm}	$a_{cdm}(412)=a_{cdm+pc}(412)$ $a_{cdm}(510)=a_{cdm+pc}(510)$ $S_{cdm}=-\frac{1}{98}\ln\frac{a_{cdm}(412)}{a_{cdm}(510)}$
10	$a_{cdm}(\lambda)$	$a_{cdm}(\lambda)=a_{cdm}(412)\exp[-S_{cdm}\times(\lambda-412)]$ and $a_{cdm}(715)$ is set to 0*.
11	$a_{ph}(\lambda)$	$a_{ph}(\lambda)=a_{t-w}(\lambda)-a_{cdm}(\lambda)$
12	$a_{pc}(620)$	$a_{pc}(620)=a_{cdm+pc}(620)-a_{cdm}(620)$
13	PC (mg m^{-3})	$\mathrm{PC}=\frac{a_{pc}(620)}{a^{*}_{pc}(620)}$, $a^{*}_{pc}(620)=0.0043$ m^2 (mg PC)$^{-1}$

* GAM-estimated $a_{t\text{-}w}(\lambda)$ shows anomalies beyond 715 nm (Chapter 2). In stead of usually forcing $a_{cdm}(750)$ to zero, $a_{cdm}(710)$ is considered as offset and thus subtracted from whole $a_{cdm}(\lambda)$, or else anomalies will occur in derived $a_{ph}(\lambda)$ as well.

The difference between algorithm developed in this study and the semi-empirical algorithm by Simis et al. (2005 & 2007) mainly includes 1) CDM absorption at 620 nm is considered when deriving $a_{pc}(620)$ in this study, but not by Simis et al. (2005 & 2007); and 2) PC absorption is an independent component and do not correlate with other pigments absorption in this study, but Simis et al. (2005 & 2007) used an empirical relationship between PC absorption and all phytoplankton pigments absorption to estimate $a_{pc}(620)$. As a result, some limitations of the semi-empirical algorithm by Simis et al. (2005 & 2007) are expected to be overcome using the new algorithm in this study.

2.6 Retrieval of phycocyanin concentration

PC concentration can be determined by dividing $a^{*}_{pc}(620)$ from $a_{pc}(620)$.

$$\mathrm{PC}(\mathrm{mg\,m^{-3}}) = \frac{a_{pc}(620)}{a^{*}_{pc}(620)} \tag{14}$$

The key to accurately predict PC is to choose an appropriate $a^{*}_{pc}(620)$. Simis et al. (2005) measured $a^{*}_{pc}(620)$ =0.0095 m^2 (mg PC)$^{-1}$ with a standard deviation of 0.0033 m^2 (mg PC)$^{-1}$, but they lowered to 0.007 m^2 (mg PC)$^{-1}$ (Simis et al. 2007). In Chapter 2, it suggested that $a^{*}_{pc}(620)$ determined for extracts of low PC is not stable because the ratio of signal to noise for $a_{pc}(620)$ is too weak due to instability of spectrophotometer. In addition, the intracellular water-soluble compounds, which is akin to sheath pigments commonly found in cyanobacteria (Subramaniam et al. 1999), impose a background on measured $a_{pc}(620)$ and thus elevate $a^{*}_{pc}(620)$. Therefore, the $a^{*}_{pc}(620)$ measured by Simis et al. (2007) are too high to determine PC in this study. Alternatively, the value measured in high PC concentration by Jupp et al. (1994) was used to determine PC, and therefore $a^{*}_{pc}(620)$ is set to 0.0043 m^2 (mg PC)$^{-1}$ in this study.

The accuracy of the estimation is evaluated by relative root mean square error (rRMSE) and relative error (RE) shown in equations 15 and 16, respectively.

$$\mathrm{rRMSE} = \frac{\sqrt{\frac{1}{n}\sum_{i=1}^{n}(X_i' - X_i)}}{\frac{1}{n}\sum_{i=1}^{n}X_i} \times 100\% \tag{15}$$

$$\mathrm{RE} = \frac{|X_i' - X_i|}{X_i} \times 100\% \tag{16}$$

where n is the total sample number, and X_i' and X_i are the estimated and measured values for sample i, respectively.

3. Results

3.1. Retrieval of $a_{ph}(\lambda)$ and $a_{cdm}(\lambda)$

The derived absorption spectra are shown in Fig. 3.5.A-5.D for $a_{cdm+pc}(\lambda)$, $a_{cdm}(\lambda)$, $a_{ph-pc}(\lambda)$ and $a_{ph}(\lambda)$, respectively. Fig. 3.5.A clearly shows $a_{cdm+pc}(\lambda)$ overall has the exponential decay trend with increased wavelength, the characteristics of CDM absorption, and the peaks due to PC and phycoerythrin (PE) are observed. The modeled $a_{cdm}(\lambda)$ based on equation 11a-11b is shown in Fig. 3.5.B and the PC and PE absorption features are completely removed. Comparison of figures 5.C and 5.D results in the difference between the $a_{ph-pc}(\lambda)$ and $a_{ph}(\lambda)$ with the latter showing phycobilins (PC and PE) absorptions and the former not. The shapes of retrieved CDM and phytoplankton absorption coefficients overall tally with the actual ones of measured absorption coefficients shown in Fig. 3.3, albeit some differences exist.

Comparison between estimated and measured absorption values at featured bands (Fig. 3.6) shows that the proposed algorithm succeeds in separating $a_{ph}(\lambda)$ and $a_{cdm}(\lambda)$ with relatively high accuracy. $a_{cdm}(443)$ is commonly used as proxy of CDM concentration, and the estimated and measured $a_{cdm}(443)$ fit well with R^2=0.844 and rRMSE=30.6%. Small underestimation is observed for six samples with $a_{cdm}(443)$ ranging between 3.6 m^{-1} and 4.6 m^{-1}. While slight underestimation for $a_{ph}(620)$ happens (R^2=0.795, rRMSE=34.3%) but no overestimation or underestimation is observed for $a_{ph}(443)$ (R^2=0.785, rRMSE = 23.1%) and $a_{ph}(675)$ (R^2=0.847, rRMSE=21.5%). In general, the estimation at all compared featured bands are accurate with estimated $a_{ph}(675)$ at the best accuracy.

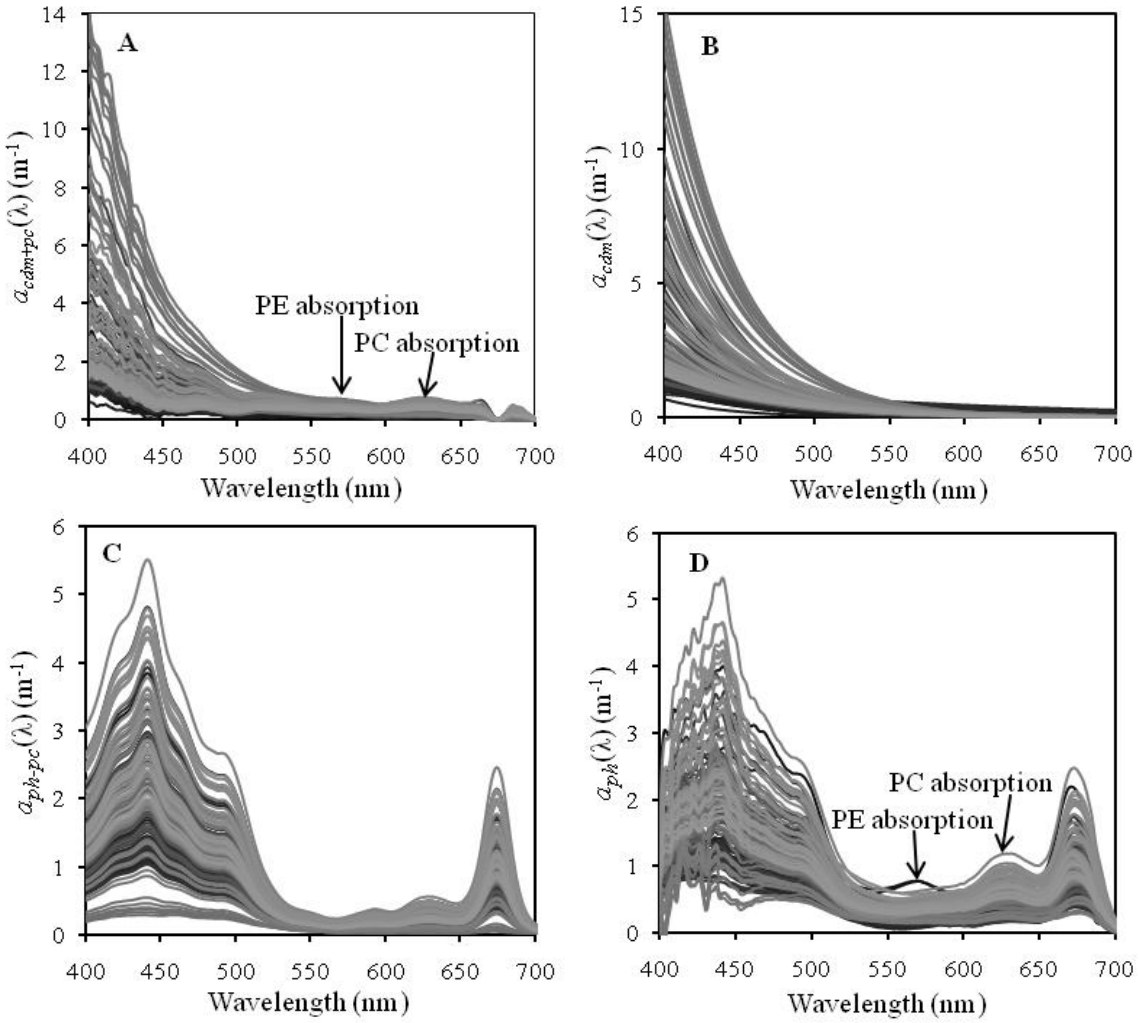

Fig. 3.5. A: retrieved $a_{cdm+pc}(\lambda)$ which includes absorption of CDM, PC, PE. PE is not soluble in acetone either. B: modeled $a_{cdm}(\lambda)$ from A. The absorption peaks of pigments, those not soluble in acetone are eliminated. C: modeled $a_{ph\text{-}pc}(\lambda)$ using equation 4 with GTM-estimated $a_{ph\text{-}pc}(675)$. D: estimated $a_{ph}(\lambda)$ which contains absorption features of all pigments.

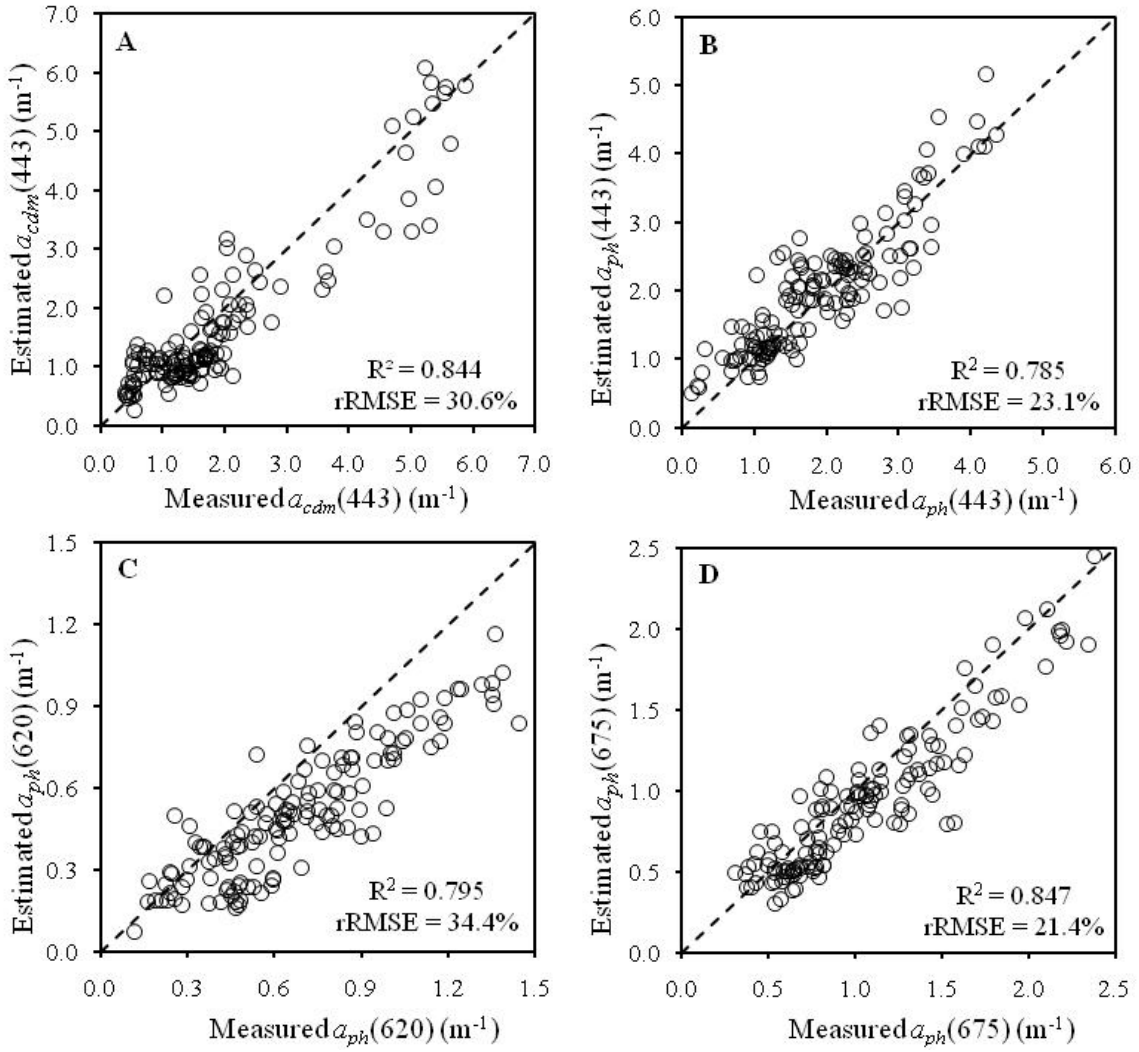

Fig. 3.6. Comparison between measured and estimated absorption coefficients for featured bands. A: estimated $a_{cdm}(443)$ vs. measured $a_{cdm}(443)$; B: estimated $a_{ph}(443)$ vs. measured $a_{ph}(443)$; C: estimated $a_{ph}(620)$ vs. measured $a_{ph}(620)$; D: estimated $a_{ph}(675)$ vs. measured $a_{ph}(675)$. Dash line represents 1:1 line.

3.2. Estimation of PC concentration

Dividing $a_{pc}(620)$ with PC specific absorption coefficient $a^*_{pc}(620)$=0.0043 m^2 (mg PC)$^{-1}$ gives rise to estimated PC concentration. The correlation between estimated and measured PC is shown in Fig. 3.7.A with R^2=0.798, rRMSE=30.6% and mean RE=40.1%.

The samples evenly distribute around the 1:1 line, and significant overestimation does not present for samples with low PC (PC≤50 mg m^{-3}). Using the semi-empirical algorithm developed by Simis et al. (2005) resulted in consistently overestimated PC for samples with PC less than 50 mg m^{-3} as indicated by the intercept 25.406 mg m^{-3} of the regression line between estimated and measured PC (Fig. 3.7.B), which is close to the intercept 29 mg m^{-3} observed by Simis et al. (2005). The mean RE for estimated PC (40.1%) with the algorithm proposed in this study is much lower than 82.0% for the semi-empirical algorithm by Simis et al. (2005 & 2007).

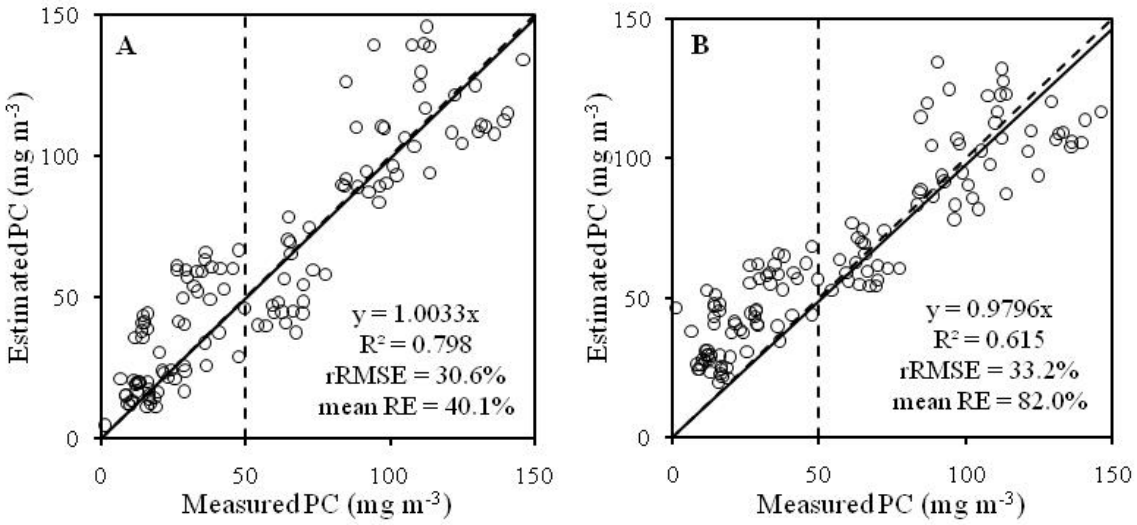

Fig. 3.7. Comparison between measured and estimated PC concentrations. A: by approach in this study; B:by semi-empirical algorithm developed by Simis et al. (2005). Dash line represents 1:1 line, and solid line is regression line.

4. Discussion

4.1. Absorption partitioning methods for inland waters

It is aforementioned that several methods (e.g. C06, O07 and W09; see section 2.5 for their brief description) are available to partition $a_{t\text{-}w}(\lambda)$ into $a_{ph}(\lambda)$ and $a_{cdm}(\lambda)$. All of them were originally developed for coastal and ocean waters and their feasibility for inland

waters were tested. Specially, Chl-*a* concentration for C06 come from the estimation of GAM (Fig. 3.8) but not the laboratory-measured Chl-*a* concentrations. The reason why the estimated Chl-*a* was chosen as input of C06 is to examine if C06 could be used to automatically derive $a_{ph}(\lambda)$ and $a_{cdm}(\lambda)$ from remote sensing reflectance without using laboratory measured data. Thereafter their performances for samples collected in three sites in Indiana, the highly eutrophic inland waters, are examined by correlating modeled and measured absorption coefficients, and compared with the performance of this study. The results are presented in table 3.5. For deriving $a_{cdm}(443)$ and $a_{ph}(443)$, W09 and O07 perform neither as well as the method proposed in this study nor well as C06. The poor performance of W09 can be attributed to its use of band 443 nm where $a_{ph}(\lambda)$ exhibits high variability, and many previous investigations using this band show the similar results (e.g. Hoge & Lyon, 1999; Hoge et al., 1999; and references therein). For O07, two pairs of fixed ratios (i. e., $a_{ph}(510)/a_{ph}(412)\approx0.435$ and $a_{ph}(555)/a_{ph}(630)\approx0.98$) may not be valid for inland waters, at least for three sites investigated in this study, which results in degradation of its performance for estimating $a_{cdm}(443)$ and $a_{ph}(443)$. Nevertheless, when taking into account the changes of $a_{ph}(\lambda)$ with Chl-*a*, e.g. this study and C06, the performances of algorithms increase significantly. Therefore, it is evident that the variability of $a_{ph}(\lambda)$ has strong effects on retrieval of $a_{cdm}(443)$ and $a_{ph}(443)$. Although the performances of different methods on estimating $a_{cdm}(443)$ and $a_{ph}(443)$ vary, derivations of $a_{ph}(675)$ by all four methods generate consistent results. This is attributed to the decreased and insignificant effect of $a_{cdm}(\lambda)$ with increased wavelength and $a_{cdm}(675)$ contributes little to $a_{ph}(675)$, leading to $a_{ph}(675)\approx a_{t\text{-}w}(675)$, as suggested by Simis et al. (2005 & 2007). With respect to derivation of $a_{ph}(620)$, errors induced by CDM

absorption have some influences but not strong as on $a_{ph}(443)$, which is the reason why C06, O07 and this study achieved comparable accuracies for $a_{ph}(620)$, but W09 estimates less accurately because W09 estimates $a_{cdm}(443)$ worst. In conclusion, both C06 and method in this study are suitable for automatically partitioning $a_{t\text{-}w}(\lambda)$, which is estimated from remote sensing reflectance, into $a_{ph}(\lambda)$ and $a_{cdm}(\lambda)$ in eutrophic inland waters, even no laboratory measured Chl-*a* concentrations available for C06.

Table 3.5. The comparison of the partitioning methods. C06=Ciotti & Bricaud et al. (2006), O07=Oubelkheir et al (2007) and W09=Wang et al. (2009).

Parameter	W09		C06		O07		This study	
	R^2	rRMSE	R^2	rRMSE	R^2	rRMSE	R^2	rRMSE
$a_{cdm}(443)$	0.460	90.2%	0.823	36.6%	0.823	51.5%	0.844	30.6%
$a_{ph}(443)$	0.563	73.8%	0.749	27.6%	0.731	46.8%	0.785	23.1%
$a_{ph}(620)$	0.639	69.8%	0.761	32.3%	0.753	32.0%	0.795	34.4%
$a_{ph}(675)$	0.848	25.6%	0.846	21.1%	0.846	21.1%	0.847	21.4%

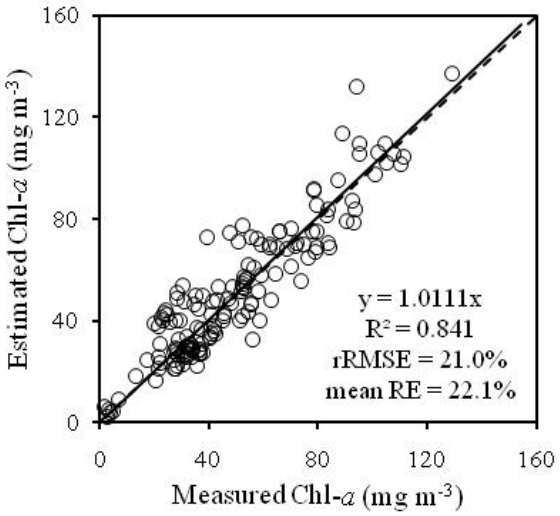

Fig. 3.8. Evaluation of the accuracy of GTM-estimated Chl-*a* vs. measured Chl-*a*. Dash line represents 1:1 line, and solid line is regression line.

However, the proposed method based on $a_{sol}(\lambda)$ has advantages over C06. The advantages come from the observation that some pigments, typically phycobilins (PE and

PC), are not soluble in organic solvent. These pigments have very weak absorption even at its maximum, and their absorption usually overlaps with those of other pigments, e.g. Chl-*a*, chlorophyll-*b* (Chl-*b*), chlorophyll-*c* (Chl-*c*), etc. (Simis et al., 2007). In fact, it is difficult to determine the contribution of each pigment to total $a_{ph}(\lambda)$, but using the method proposed in this paper can at least determines the absorption maximums of water-soluble and acetone-soluble pigments. For example, Fig. 3.5.A shows the absorption peaks due to PE and PC after removing the absorption of acetone-soluble pigments, and the corresponding depression features on $r_{rs}(\lambda)$ are shown in Fig. 3.1. Furthermore it is successful to use $a_{pc}(620)$ extracted from $a_{cdm+pc}(\lambda)$ for estimation of PC concentration, and it might be feasible to estimate the concentrations of more accessory pigments, if individual pigment absorption is represented by a function of its absorption maximum so that $a_{ph\text{-}pc}(\lambda)$ can be further decomposed into individual components for different pigments.

4.2. Factors influencing the estimation of PC

As indicated above, the contribution of $a_{cdm}(620)$ to $a_{ph}(620)$ can leads to significant overestimation of low PC (PC≤50 mg m^{-3}) (see Fig. 3.7, section 1 and section 3.2). Particularly, the mean RE for estimated PC (40.1%) in this study is much lower than RE (82.0%) observed for the semi-empirical algorithm by Simis et al. (2005 & 2007). This improvement by this study evidently suggests that the influence of $a_{cdm}(620)$ on the PC estimation is effectively eliminated, and thus CDM becomes not significant for PC estimation by our algorithm.

In addition to the effect of the CDM absorption, the ratio of PC to Chl-*a* (PC:Chl-*a*) can also interfere the estimation of PC because Chl-*a* and accessory pigments (Chl-*b* and

Chl-*c*) all contribute to the absorption at 620 nm (Simis et al., 2007). Both Fig. 3.9.A and Fig. 3.9.B show when PC:Chl-*a* is less than 0.5, RE (equation 15) for estimated PC increases significantly, which is due to failure of using fixed fraction 0.24 in $a_{pc}(620)=a_{ph}(620)-0.24a_{ph}(665)$ and was also observed by Hunter et al. (2010). In this study, the $a_{ph\text{-}pc}(\lambda)$ measurement of was conducted for water samples collected through three different seasons from April to October and having a wide range of Chl-*a* from 1.85 mg m^{-3} to 136.95 mg m^{-3} and PC from 1.46 mg m^{-3} to 146.10 mg m^{-3}. The pigment composition found in these water samples may be expected to be representative for natural inland waters. Based on the high correlation between estimated and measured PC, it is concluded that the approach in this study evidently removes the contribution of the Chl-*a*, *b* and *c* absorptions to the PC absorption at 620 nm. In addition, RE of estimated PC by this study for most samples with PC:Chl-$a\leq0.5$ (Fig. 3.9.A) is generally lower than that (Fig. 3.9.B) resulting from the method by Simis et al. (2005). This is important because a PC:Chl-*a* value less than 0.5 indicates that cyanobacteria are not dominant (Hunter et al., 2010). The improved accuracy for prediction of PC at a low concentration significantly benefit the purpose of issue early warning for the presence of cyanobacterial blooms, which is important to protect animal and human health (Hunter et al. 2009).

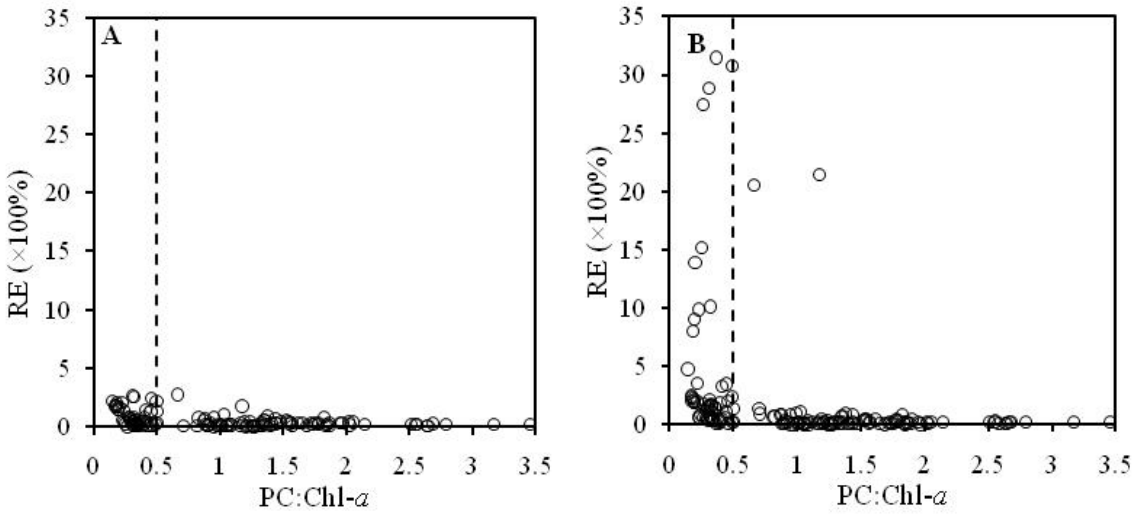

Fig. 3.9. The relationship between relative error (RE; equation 15) and PC:Chl-*a*. A: RE for the estimation by approach in this study; B: RE for the estimation by semi-empirical algorithm developed by Simis et al. (2005).

4.3. Application on simulated MERIS reflectance

The MERIS image spectra were simulated by resampling field measured reflectance spectra (Fig. 3.10.A). Fig. 3.10.B and Fig. 3.10.C show the estimated $a_{cdm}(\lambda)$ and $a_{ph}(\lambda)$ from simulated MERIS image spectra shown in Fig. 3.10.A. Fig. 3.10.D indicates that PC is accurately estimated though reducing spectral resolution from 1 nm to 10 nm results in a slightly lower R^2 (=0.754) and higher rRMSE (=32.6%) comparing to Fig. 3.7.A. The estimation for PC≤50 mg m^{-3} is still accurate. The revisit period of the MERIS satellite is 3 days, which is enough temporal resolution for tracking the dynamics of PC as well as cyanobacterial biomass growth. The algorithm described in this paper shows the capability to estimate low PC, and will be tested with the time-series of MERIS imagery to construct a cyanobacterial blooms warning system.

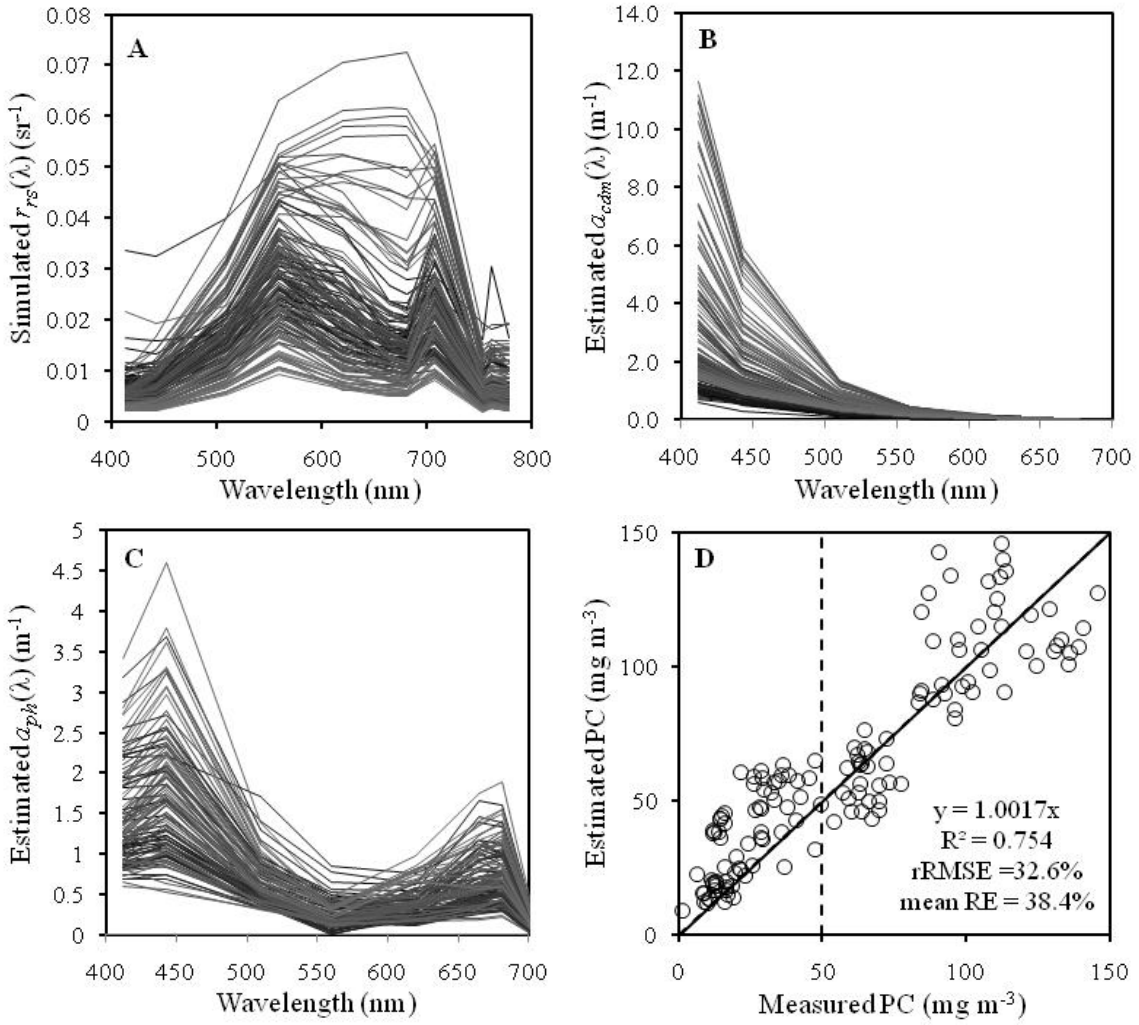

Fig. 3.10. Results based on simulation of MERIS reflectance from hyperspectral measurements. A: simulated MERIS remote sensing reflectance; B: estimated $a_{cdm}(\lambda)$; C: estimated $a_{ph}(\lambda)$; D: estimated PC vs. measured PC.

5. Conlusions

A new absorption coefficients partitioning method, by the aid of absorption coefficients of acetone-extracted pigments, is proposed to derive phytoplankton and CDM absorption spectra from GAM-estimated $a_{t\text{-}w}(\lambda)$. Accurate estimation is achieved for the partitioned $a_{cdm}(\lambda)$ and $a_{ph}(\lambda)$ through the quantitative evaluation at several featured bands, e.g. R^2=0.844 for $a_{cdm}(443)$, R^2=0.785 for $a_{ph}(443)$, R^2=0.795 for $a_{ph}(620)$

and R^2=0.847 for a_{ph}(675), respectively. Meanwhile, PC absorption at 620 nm was derived by considering it as an independent component in the partitioning process, and then PC concentrations were retrieved from a_{pc}(620) with R^2=0.798 and rRMSE=30.6%. Particularly, no significant overestimation was observed for samples of low PC concentration (e.g. PC≤50 mg m^{-3}), which is commonly the case of semi-empirical algorithm. The improvement is evidently due to elimination of CDM absorption and consideration of pigment composition. In addition, both Chl-*a* and PC concentrations span a range from ~1.5 mg m^{-3} to ~150 mg m^{-3} usually observed in eutrophic inland waters in different seasons. Therefore, the method is suggested to be suitable for detection of PC in inland waters unless algal scum emerges on the water surface, and it is not necessary that cyanobacteria are the dominant phytoplankton species. Particularly, accurate estimation based on simulated MERIS reflectance spectra implies the feasibility of routinely surveillance of cyanobacterial biomass dynamics in the future, based on which a system can be established to warn potential risks of cyanobacterial population growth to the public.

Acknowledgements

The authors thank Center of Earth and Environmental Sciences (CEES), Indiana University-Purdue University at Indianapolis (IUPUI), for assisting field sampling, and we thank Shuai Li, Tingting Zhang, Dawei Liu and Ying Sun for helping analyze water samples. The fund support (Grant No. NNX09AU87G) by the NASA Energy and Water Cycle Study program is appreciated.

IV. CONCLUSIONS

In this thesis, a bio-optical model was developed to retrieve inherent optical properties based on Chl-*a* and PC concentrations. The results show that the predicted $a_{t\text{-}w}(440)$ and $a_{t\text{-}w}(675)$ fit very well with measured ones, while $a_{t\text{-}w}(550)$ is significantly underestimated, which is probably due to negligibility of the quadratic term of reflectance model in Gordons et al. (1988). Because $a_{cdm}(\lambda)$ has only minor impacts on $a_{t\text{-}w}(\lambda)$ at long wavelengths, Chl-*a* concentration was calculated using laboratory-derived Chl-*a* equation (Ritchie, 2008) based on GAM-estimated $a_{t\text{-}w}(\lambda)$ and was accurately retrieved for all study sites. In fact, the successful application of equation in Ritchie (2008) is primarily due to the stability of $a^*_{ph}(665)$ over global case 2 waters, because accuracy of Chl-*a* estimation is mainly determined by estimation of $a_{ph}(665)$. Both Gons et al. (2008) and this study observed the same $a^*_{ph}(665)$ (=0.016 m^2 (mg^{-1} Chl-*a*)) which should be suitable for global inland waters. The establishment of a common value for $a^*_{ph}(665)$ in global inland waters will drive the development of algorithms for Chl-*a*, e.g. equation 24 enables the routine retrieval of Chl-*a* concentration using MERIS imagery.

Unlike Chl-*a*, PC absorption is significantly influenced by CDM and other pigments, and thus PC concentration cannot be estimated from $a_{t\text{-}w}(\lambda)$. An innovative method, based on the fact that PC is not soluble in acetone while other pigments are, was developed to separate $a_{cdm}(\lambda)$ and $a_{ph}(\lambda)$ and to derive $a_{pc}(620)$. It demonstrates that $a_{cdm}(\lambda)$ and $a_{ph}(\lambda)$ were successfully and accurately predicted from GAM-estimated $a_{t\text{-}w}(\lambda)$. Subsequently, $a_{pc}(620)$ and PC concentration were estimated for a data set collected from three reservoirs in Indiana, 2010. Although relative errors are still relatively high when cyanobacteria do not dominate phytoplankton species, the accuracy is dramatically

improved compared to the most widely used semi-empirical model developed by Simis et al. (2007). Further improvements are required to enable its use for an early warning system for cyanobacterial population growth in the early stages.

To investigate the spatial and temporal transferability, the model was applied to data sets collected both spatially and annually without specific calibration. It evidently supports that GAM performs equivalently well in each site and each season, except for a slight underestimation for some samples collected from Australia, 2009. Therefore, GAM shows good spatiotemporal transferability for estimating Chl-*a* and PC concentrations. This actually indicates the strong capability of GAM for routinely monitoring cyanobacterial blooms.

REFERENCES

Allali, K., Bricaud, A., & Claustre, H. (1997). Spatial variations in the chlorophyll-specific absorption coefficients of phytoplankton and photosynthetically active pigments in the equatorial Pacific. *Journal of Geophysical Research-Oceans, 102*, 12413-12423.

Arar, E.J., & Collins, G.B. (1997). *In vitro* determination of chlorophyll a and pheophytin a in marine and freshwater algae by fluorescence (Method 445.0, Revision 1.2). Cincinnati, Ohio: U. S. Environmental Protection Agency. http://www.epa.gov/microbes/m445_0.pdf.

Backer, L.C. (2002). Cyanobacterial harmful algal blooms (CyanoHABs): Developing a public health response. *Lake and Reservoir Management, 18*, 20-31.

Baker, P.D., Brookes, J.D., Burch, M.D., Maier, H.R., & Ganf, G.G. (2000). Advection, growth and nutrient status of phytoplankton populations in the lower River Murray, South Australia. *Regulated Rivers-Research & Management, 16*, 327-344.

Brando, V.E., & Dekker, A.G. (2003). Satellite hyperspectral remote sensing for estimating estuarine and coastal water quality. *Ieee Transactions on Geoscience and Remote Sensing, 41*, 1378-1387.

Bricaud, A., Babin, M., Morel, A., & Claustre, H. (1995). Variability in the Chlorophyll-Specific Absorption-Coefficients of Natural Phytoplankton - Analysis and Parameterization. *Journal of Geophysical Research-Oceans, 100*, 13321-13332.

Bricaud, A., Morel, A., & Prieur, L. (1981). Absorption by dissolved organic matter of the sea (yellow substance) in the UV and visible domain. *Limnology and Oceanography, 26*, 43-53.

Bricaud, A., & Stramski, D. (1990). Spectral absorption coefficients of living phytoplankton and nonalgal biogenous matter: a comparison between the Peru upwelling area and the Sargasso Sea. *Limnology and Oceanography, 35*, 562-582.

Budd, J.W., & Warrington, D.S. (2004). Satellite-based sediment and chlorophyll a estimates for Lake Superior. *Journal of Great Lakes Research, 30*, 459-466.

Buiteveld, H., Hakvoort, J.H.M., & Donze, M. (1994). The optical properties of pure water. *SPIE Proc. Ocean Optics XII, 2258*, 174-183.

Bukata, R.P. (1995). *Optical properties and remote sensing of inland and coastal waters*. Boca Raton, Fla.: CRC Press.

Burch, M.D., Steffenson, D.A., Bursill, D.B., Bain, D.B., Ganf, G.B., & Brookes, J.D. (1994). Critical flow and blooms of the cyanobacterium Anabaena circinalis in the Murray River system. In, *Environmental Flows* (pp. 44-51). Canberra: Australian Water and Wastewater Association.

Ciotti, A.M., & Bricaud, A. (2006). Retrievals of a size parameter for phytoplankton and spectral light absorption by colored detrital matter from water-leaving radiances at SeaWiFS channels in a continental shelf region off Brazil. *Limnology and Oceanography-Methods, 4*, 237-253.

Codd, G.A., Chorus, I., & Burch, M.D. (1999). Design of monitoring programmes. In I. Chorus & J. Bartram (Eds.), *Toxic cyanobacteria in water: a guide to their public health consequences, monitoring and management* (p. 416). London and New York: WHO and E&FN Spon.

Dall'Olmo, G., & Gitelson, A.A. (2005). Effect of bio-optical parameter variability on the remote estimation of chlorophyll-a concentration in turbid productive waters: experimental results (vol 44, pg 412, 2005). *Applied Optics, 44*, 3342-3342.

Dekker, A.G. (1993). Detection of optical water quality parameters for eutrophic waters by high resolution remote sensing. In. Amsterdam, The Netherland: Vrije University.

Doxaran, D., Cherukuru, N., & Lavender, S.J. (2006). Apparent and inherent optical properties of turbid estuarine waters: measurements, empirical quantification relationships, and modeling. *Applied Optics, 45*, 2310-2324.

Duan, H.T., Ma, R., Zhang, Y., Loiselle, S.A., Xu, J., Zhao, C., Zhou, L., & Shang, L. (2010). A new three-band algorithm for estimating chlorophyll concentrations in turbid inland lakes. *Environmental Research Letters, 5*, 044009 (044006pp) 10.1088/1748-9326/5/4/044009.

Emerson, R., & Lewis, M.R. (1942). The photosynthetic efficiency of phycocyanin in Chroococcus, and the problem of carotenoid participation in photosynthesis. *The Journal of General Physiology, 25*, 579-595.

Gallegos, C.L., Jordan, T.E., Hines, A.H., & Weller, D.E. (2005). Temporal variability of optical properties in a shallow, eutrophic estuary: Seasonal and interannual variability. *Estuarine Coastal and Shelf Science, 64*, 156-170.

Garver, S.A., & Siegel, D.A. (1997). Inherent optical property inversion of ocean color spectra and its biogeochemical interpretation .1. Time series from the Sargasso Sea. *Journal of Geophysical Research-Oceans, 102*, 18607-18625.

Giardino, C., Brando, V.E., Dekker, A.G., Strombeck, N., & Candiani, G. (2007). Assessment of water quality in Lake Garda (Italy) using Hyperion. *Remote Sensing of Environment, 109*, 183-195.

Gitelson, A. (1992). The peak near 700 nm on radiance spectra of algae and water - relationships of its magnitude and position with chlorophyll concentration. *International Journal of Remote Sensing, 13*, 3367-3373.

Gitelson, A.A., Dall'Olmo, G., Moses, W., Rundquist, D.C., Barrow, T., Fisher, T.R., Gurlin, D., & Holz, J. (2008). A simple semi-analytical model for remote estimation of chlorophyll-a in turbid waters: Validation. *Remote Sensing of Environment, 112*, 3582-3593.

Gitelson, A.A., Gurlin, D., Moses, W.J., & Barrow, T. (2009). A bio-optical algorithm for the remote estimation of the chlorophyll-a concentration in case 2 waters. *Environmental Research Letters, 4*, 045003.

Gitelson, A.A., Schalles, J.F., & Hladik, C.M. (2007). Remote chlorophyll-a retrieval in turbid, productive estuaries: Chesapeake Bay case study. *Remote Sensing of Environment, 109*, 464-472

Gons, H.J. (1999). Optical teledetection of chlorophyll a in turbid inland waters. *Environmental Science & Technology, 33*, 1127-1132.

Gons, H.J., Auer, M.T., & Effler, S.W. (2008). MERIS satellite chlorophyll mapping of oligotrophic and eutrophic waters in the Laurentian Great Lakes. *Remote Sensing of Environment, 112*, 4098-4106.

Gons, H.J., Rijkeboer, M., Bagheri, S., & Ruddick, K.G. (2000). Optical teledetection of chlorophyll a in estuarine and coastal waters. *Environmental Science & Technology, 34*, 5189-5192.

Gons, H.J., Rijkeboer, M., & Ruddick, K.G. (2002). A chlorophyll-retrieval algorithm for satellite imagery (Medium Resolution Imaging Spectrometer) of inland and coastal waters. *Journal of Plankton Research, 24*, 947-951.

Gons, H.J., Rijkeboer, M., & Ruddick, K.G. (2005). Effect of a waveband shift on chlorophyll retrieval from MERIS imagery of inland and coastal waters. *Journal of Plankton Research, 27*, 125-127.

Gordon, H.R., Brown, O.B., Evans, R.H., Brown, J.W., Smith, R.C., Baker, K.S., & Clark, D.K. (1988). A semianalytic radiance model of ocean color. *Journal of Geophysical Research-Atmospheres, 93*, 10909-10924.

Gould, R.W., Arnone, R.A., & Sydor, M. (2001). Absorption, scattering; and remote-sensing reflectance relationships in coastal waters: Testing a new inversion algorithm. *Journal of Coastal Research, 17*, 328-341.

Gower, J., & King, S. (2007). Validation of chlorophyll fluorescence derived from MERIS on the west coast of Canada. *International Journal of Remote Sensing, 28*, 625-635.

Guanter, L., Ruiz-Verdu, A., Odermatt, D., Giardino, C., Simis, S., Estelles, V., Heege, T., Dominguez-Gomez, J.A., & Moreno, J. (2010). Atmospheric correction of ENVISAT/MERIS data over inland waters: Validation for European lakes. *Remote Sensing of Environment, 114*, 467-480.

Hakvoort, H., de Haan, J., Jordans, R., Vos, R., Peters, S., & Rijkeboer, M. (2002). Towards airborne remote sensing of water quality in The Netherlands - validation and error analysis. *Isprs Journal of Photogrammetry and Remote Sensing, 57*, 171-183.

Hoge, F.E., & Lyon, P.E. (1996). Satellite retrieval of inherent optical properties by linear matrix inversion of oceanic radiance models: An analysis of model and radiance measurement errors. *Journal of Geophysical Research-Oceans, 101*, 16631-16648.

Hoge, F.E., & Lyon, P.E. (1999). Spectral parameters of inherent optical property models: method for satellite retrieval by matrix inversion of an oceanic radiance model. *Applied Optics, 38*, 1657-1662.

Hoge, F.E., & Lyon, P.E. (2005). New tools for the study of oceanic eddies: Satellite derived inherent optical properties. *Remote Sensing of Environment, 95*, 444-452.

Hoge, F.E., Wright, C.W., Lyon, P.E., Swift, R.N., & Yungel, J.K. (1999a). Satellite retrieval of inherent optical properties by inversion of an oceanic radiance model: a preliminary algorithm. *Applied Optics, 38*, 495-504.

Hoge, F.E., Wright, C.W., Lyon, P.E., Swift, R.N., & Yungel, J.K. (1999b). Satellite retrieval of the absorption coefficient of phytoplankton phycoerythrin pigment: theory and feasibility status. *Applied Optics, 38*, 7431-7441.

Hoogenboom, H.J., Dekker, A.G., & de Haan, J.F. (1998). Retrieval of chlorophyll and suspended matter from imaging spectrometry data by matrix inversion. *Canadian Journal of Remote Sensing, 24*, 144-152.

Hu, C.M. (2009). A novel ocean color index to detect floating algae in the global oceans. *Remote Sensing of Environment, 113*, 2118-2129.

Hu, C.M., Muller-Karger, F.E., Taylor, C., Carder, K.L., Kelble, C., Johns, E., & Heil, C.A. (2005). Red tide detection and tracing using MODIS fluorescence data: A regional example in SW Florida coastal waters. *Remote Sensing of Environment, 97*, 311-321.

Hunter, P.D., Tyler, A.N., Carvalho, L., Codd, G.A., & Maberly, S.C. (2010). Hyperspectral remote sensing of cyanobacterial pigments as indicators for cell populations and toxins in eutrophic lakes. *Remote Sensing of Environment, 114*, 2705-2718.

Hunter, P.D., Tyler, A.N., Gilvear, D.J., & Willby, N.J. (2009). Using remote sensing to aid the assessment of human health risks from blooms of potentially toxic cyanobacteria. *Environmental Science & Technology, 43*, 2627-2633.

Hunter, P.D., Tyler, A.N., Willby, N.J., & Gilvear, D.J. (2008). The spatial dynamics of vertical migration by Microcystis aeruginosa in a eutrophic shallow lake: A case study using high spatial resolution time-series airborne remote sensing. *Limnology and Oceanography, 53*, 2391-2406.

IOCCG (2006). Remote sensing of inherent optical properties: Fundamentals, tests of algorithms, and application. In Z.P. Lee (Ed.). Dartmouth, Canada: IOCCG.

Jupp, D.L.B., Kirk, J.T.O., & Harris, G.P. (1994). Detection, identification and mapping of cyanobacteria - using remote-sensing to measure the optical-quality of turbid inland waters. *Australian Journal of Marine and Freshwater Research, 45*, 801-828.

Kallio, K., Kutser, T., Hannonen, T., Koponen, S., Pulliainen, J., Vepsalainen, J., & Pyhalahti, T. (2001). Retrieval of water quality from airborne imaging spectrometry of various lake types in different seasons. *Science of the Total Environment, 268*, 59-77.

Kutser, T. (2004). Quantitative detection of chlorophyll in cyanobacterial blooms by satellite remote sensing. *Limnology and Oceanography, 49*, 2179-2189.

Kutser, T., Metsamaa, L., Strombeck, N., & Vahtmae, E. (2006). Monitoring cyanobacterial blooms by satellite remote sensing. *Estuarine Coastal and Shelf Science, 67*, 303-312.

Le, C.F., Li, Y.M., Zha, Y., Sun, D.Y., Huang, C.C., & Lu, H. (2009a). A four-band semi-analytical model for estimating chlorophyll a in highly turbid lakes: The case of Taihu Lake, China. *Remote Sensing of Environment, 113*, 1175-1182.

Le, C.F., Li, Y.M., Zha, Y., Sun, D.Y., Huang, C.C., & Zhang, H. (2011). Remote estimation of chlorophyll a in optically complex waters based on optical classification. *Remote Sensing of Environment, 115*, 725-737.

Le, C.F., Li, Y.M., Zha, Y., Sun, D.Y., & Yin, B. (2009b). Validation of a quasi-analytical algorithm for highly turbid eutrophic water of Meiliang Bay in Taihu Lake, China. *Ieee Transactions on Geoscience and Remote Sensing, 47*, 2492-2500.

Lee, Z., Weidemann, A., Kindle, J., Arnone, R., Carder, K.L., & Davis, C. (2007). Euphotic zone depth: Its derivation and implication to ocean-color remote sensing. *Journal of Geophysical Research-Oceans, 112*, - 10.1029/2006JC003802.

Lee, Z.P., & Carder, K.L. (2004). Absorption spectrum of phytoplankton pigments derived from hyperspectral remote-sensing reflectance. *Remote Sensing of Environment, 89*, 361-368.

Lee, Z.P., Carder, K.L., & Arnone, R.A. (2002). Deriving inherent optical properties from water color: a multiband quasi-analytical algorithm for optically deep waters. *Applied Optics, 41*, 5755-5772.

Lee, Z.P., Carder, K.L., Mobley, C.D., Steward, R.G., & Patch, J.S. (1999). Hyperspectral remote sensing for shallow waters: 2. Deriving bottom depths and water properties by optimization. *Applied Optics, 38*, 3831-3843.

Lee, Z.P., Carder, K.L., Peacock, T.G., Davis, C.O., & Mueller, J.L. (1996). Method to derive ocean absorption coefficients from remote-sensing reflectance. *Applied Optics, 35*, 453-462.

Lee, Z.P., Lubac, B., Werdell, J., & Arnone, R. (2009). An update of the quasi-analytical algorithm (v5). IOCCG software report. www.ioccg.org/groups/Software_OCA.

Li, L., Sengpiel, R.E., Pascual, D.L., Tedesco, L.P., Wilson, J.S., & Soyeux, E. (2010). Using hyperspectral remote sensing to estimate chlorophyll-a and phycocyanin in a mesotrophic reservoir. *International Journal of Remote Sensing, 31*, 4147-4162.

Lorenzen, C.J. (1967). Determination of chlorophyll and pheo-pigments: spectrophotometric equations. *Limnology and Oceanography, 12*, 343-346.

Lu, D.M., Song, K.S., Li, L., Liu, D.W., Li, S., Wang, Y.D., Wang, Z.M., Xu, J.P., & M., J.M. (2010). Training a GA-PLS model for Chl-a concentration estimation over inland lake in Northest China. *Procedia Environmental Science, 2*, 842-851.

Maier, H.R., Dandy, G.C., & Burch, M.D. (1998). Use of artificial neural networks for modeling cyanobacteria *Anabaena* spp. in the River Murray, South Australia. *Ecological Modeling, 105*, 257-272.

Mao, Z.H., Stuart, V., Pan, D.L., Chen, J.Y., Gong, F., Huang, H.Q., & Zhu, Q.K. (2010). Effects of phytoplankton species composition on absorption spectra and modeled hyperspectral reflectance. *Ecological Informatics, 5*, 359-366.

Maritorena, S., & Siegel, D.A. (2005). Consistent merging of satellite ocean color data sets using a bio-optical model. *Remote Sensing of Environment, 94*, 429-440.

Maritorena, S., & Siegel, D.A. (2006). The GSM semi-analytical bio-optical model. In Z.P. Lee (Ed.), *Remote sensing of inherent optical properties, fundamentals, tests of algorithms, and applications* (pp. 81-86). Dartmous, Canada.

Maritorena, S., Siegel, D.A., & Peterson, A.R. (2002). Optimization of a semianalytical ocean color model for global-scale applications. *Applied Optics, 41*, 2705-2714.

Matthews, M.W., Bernard, S., & Winter, K. (2010). Remote sensing of cyanobacteria-dominant algal blooms and water quality parameters in Zeekoevlei, a small hypertrophic lake, using MERIS. *Remote Sensing of Environment, 114*, 2070-2087.

Metsamaa, L., Kutser, T., & Strombeck, N. (2006). Recognising cyanobacterial blooms based on their optical signature: a modelling study. *Boreal Environment Research, 11*, 493-506.

Mishra, S., Mishra, D.R., & Schluchter, W.M. (2009). A novel algorithm for predicting phycocyanin concentrations in cyanobacteria: a proximal hyperspectral remote sensing approach. *Remote Sensing, 1*, 758-775 doi:10.3390/rs1040758.

Mobley, C.D. (1999). Estimation of the remote-sensing reflectance from above-surface measurements. *Applied Optics, 38*, 7442-7455.

Morel, A., & Gentili, B. (1993). Diffuse-Reflectance of Oceanic Waters .2. Bidirectional Aspects. *Applied Optics, 32*, 6864-6879.

Morel, A., & Gentili, B. (1996). Diffuse reflectance of oceanic waters .3. Implication of bidirectionality for the remote-sensing problem. *Applied Optics, 35*, 4850-4862.

Morel, A., & Maritorena, S. (2001). Bio-optical properties of oceanic waters: A reappraisal. *Journal of Geophysical Research-Oceans, 106*, 7163-7180.

Muerller, J.L., & Fargion, G.S. (2002). Ocean optics protocols for satellite ocean color sensor validation, Revision 3, *2*, 171-179.

Myers, J., & Kratz, W.A. (1955). Relations between pigment content and photosynthetic characteristics in a blue-green alga. *The Journal of General Physiology, 39*, 11-22.

O'Reilly, J.E., Maritorena, S., Mitchell, B.G., Siegel, D.A., Carder, K.L., Garver, S.A., Kahru, M., & McClain, C. (1998). Ocean color chlorophyll algorithms for SeaWiFS. *Journal of Geophysical Research-Oceans, 103*, 24937-24953.

Oubelkheir, K., Claustre, H., Bricaud, A., & Babin, M. (2007). Partitioning total spectral absorption in phytoplankton and colored detrital material contributions. *Limnology and Oceanography-Methods, 5*, 384-395.

Paerl, H.W., & Huisman, J. (2009). Climate change: a catalyst for global expansion of harmful cyanobacterial blooms. *Environmental Microbiology Reports, 1*, 27-37.

Randolph, K., Wilson, J., Tedesco, L., Li, L., Pascual, D.L., & Soyeux, E. (2008). Hyperspectral remote sensing of cyanobacteria in turbid productive water using optically active pigments, chlorophyll a and phycocyanin. *Remote Sensing of Environment, 112*, 4009-4019.

Richardson, L.L. (1996). Remote sensing of algal bloom dynamics. *Bioscience, 46*, 492-501.

Ritchie, R.J. (2008). Universal chlorophyll equations for estimating chlorophylls a, b, c, and d and total chlorophylls in natural assemblages of photosynthetic organisms using acetone, methanol, or ethanol solvents. *Photosynthetica, 46*, 115-126.

Ruiz-Verdu, A., Simis, S.G.H., de Hoyos, C., Gons, H.J., & Pena-Martinez, R. (2008). An evaluation of algorithms for the remote sensing of cyanobacterial biomass. *Remote Sensing of Environment, 112*, 3996-4008.

Salama, M.S., Dekker, A., Su, Z., Mannaerts, C.M., & Verhoef, W. (2009). Deriving inherent optical properties and associated inversion-uncertainties in the Dutch Lakes. *Hydrology and Earth System Sciences, 13*, 1113-1121.

Sarada, R., Pillai, M.G., & Ravishankar, G.A. (1999). Phycocyanin from Spirulina sp: influence of processing of biomass on phycocyanin yield, analysis of efficacy of extraction methods and stability studies on phycocyanin. *Process Biochemistry, 34*, 795-801.

Sathyendranath, S., Prieur, L., & Morel, A. (1989). A three-component model of ocean colour and its application to remote sensing of phytoplankton pigments in coastal waters. *International Journal of Remote Sensing, 10*, 1373-1394.

Schalles, J. (2006). Optical remote sensing techniques to estimate phytoplankton chlorophyll a coencentrations in coastal waters with varying suspended matter and CDOM concentrations. In L.L. Richardson & E.F. LeDrew (Eds.), *Remote sensing of aquatic coastal ecosystem process: Science and management applications* (pp. pp. 27-79): Springer.

Schalles, J., Rundquist, D.C., & Schiebe, F.R. (2001). The influence of suspended clays on phytoplankton reflectance signatures and the remote sensing of chlorophyll. *Vehr. Intern. Verein. Limnol., 27*, 3619-3625.

Schalles, J.F., & Yacobi, Y.Z. (2000). Remote detection and seasonal patterns of phycocyanin, carotenoid and chlorophyll pigments in eutrophic waters. *Archiv für Hydrobiologie Special Issues Advances in Limnology, 55*, 153-168.

Shibata, K., Benson, A.A., & Calvin, M. (1954). The absorption spectra of suspensions of living micro-organisms. *Biochimica ET Biophysica Acta, 15*, 461-470.

Simis, S.G.H., Peters, S.W.M., & Gons, H.J. (2005). Remote sensing of the cyanobacterial pigment phycocyanin in turbid inland water. *Limnology and Oceanography, 50*, 237-245.

Simis, S.G.H., Ruiz-Verdu, A., Dominguez-Gomez, J.A., Pena-Martinez, R., Peters, S.W.M., & Gons, H.J. (2007). Influence of phytoplankton pigment composition on remote sensing of cyanobacterial biomass. *Remote Sensing of Environment, 106*, 414-427.

Subramaniam, A., Carpenter, E.J., Karentz, D., & Falkowski, P.G. (1999). Bio-optical properties of the marine diazotrophic cyanobacteria Trichodesmium spp. I. Absorption and photosynthetic action spectra. *Limnology and Oceanography, 44*, 608-617.

Sun, D.Y., Li, Y.M., Wang, Q., Lv, H., Le, C.F., Huang, C.C., & Gong, S.Q. (2010). Partitioning particulate scattering and absorption into contributions of phytoplankton and non-algal particles in winter in Lake Taihu (China). *Hydrobiologia, 644*, 337-349.

Vincent, R.K., Qin, X.M., McKay, R.M.L., Miner, J., Czajkowski, K., Savino, J., & Bridgeman, T. (2004). Phycocyanin detection from LANDSAT TM data for mapping cyanobacterial blooms in Lake Erie. *Remote Sensing of Environment, 89*, 381-392.

Wang, G.F., Cao, W.X., Yang, D.T., & Zhao, J. (2009). Decomposing total suspended particle absorption based on the spectral correlation relationship. *Spectroscopy and Spectral Analysis, 29*, 201-206.

Wang, G.F., Cao, W.X., Yang, Y.Z., Zhou, W., Liu, S., & Yang, D.T. (2010). Variations in light absorption properties during a phytoplankton bloom in the Pearl River estuary. *Continental Shelf Research, 30*, 1085-1094.

Wang, P., Boss, E.S., & Roesler, C. (2005). Uncertainties of inherent optical properties obtained from semianalytical inversions of ocean color. *Applied Optics, 44*, 4074-4085.

Xu, J.P., Li, F., Zhang, B., Song, K.S., Wang, Z.M., Liu, D.W., & Zhang, G.X. (2009). Estimation of chlorophyll-a concentration using field spectral data: a case study in inland Case-II waters, North China. *Environmental Monitoring and Assessment, 158*, 105-116.

Yang, D.T., & Pan, D.L. (2006). Hyperspectral retrieval model of phycocyanin in case II waters. *Chinese Science Bulletin, 51*, 149-153.

Zhang, Y.L., Liu, M.L., van Dijk, M.A., Zhu, G.W., Gong, Z.J., Li, Y.L., & Qin, B.Q. (2009a). Measured and numerically partitioned phytoplankton spectral absorption coefficients in inland waters. *Journal of Plankton Research, 31*, 311-323.

Zhang, Y.L., Liu, M.L., Wang, X., Zhu, G.W., & Chen, W.M. (2009b). Bio-optical properties and estimation of the optically active substances in Lake Tianmuhu in summer. *International Journal of Remote Sensing, 30*, 2837-2857.

Zhou, G., Tang, J., Tian, G., Li, J., & Liu, Q. (2009). Uncerteinty analysis of inland water quality remote sensing: A review. *Advances in Earth Science, 24*, 150-158.

CURRICULUM VITAE

Linhai Li

Education:

Indiana University-Purdue University Indianapolis, Indianapolis (USA), Earth Sciences
Master of Science, August 2011

Wuhan University, Wuhan (China), Geographic Information System
Bachelor of Science, July 2009

Presentations:

Li, L., Li, L., & Song, K. (2010). A bio-optical approach to estimating chlorophyll-a concentration from hyperspectral remote sensing. SPIE Optics Application and Engineering, August 1 - 5 2010, San Diego, CA.

Publications and manuscripts:

Li, L., Qu, L., Ying, S., Liang, D., & Hu, Z. (2009). Use of Google SketchUp to implement 3D dynamic visualization. *Proc. SPIE Vol. 7492*, 74920Y.

Li, L., Li, L., & Song, K. (2010). Bio-optical approach to estimating Chlorophyll-a concentration from hyperspectral remote sensing. *Proc. SPIE Vol. 7809,* 78090E.

Li. L., Li, L., Song, K., Li, Y., Shi, K., & Li, Z. An improved analytical algorithm for remote estimation of chlorophyll-a in highly turbid waters. *Environmental Research Letters*, in review.

Li, L., Li, L., Song, K., Li, Y., Tedesco, L. P., Shi, K., & Li, Z. A globally transferable model for inland waters (I): deriving inherent optical properties and quantifying chlorophyll-a. *Remote Sensing of Environment*, in review.

Li, L., Li, L., Shi, K., Song, K., & Li, Z. A globally transferable model for inland waters (II): partitioning non-water absorption coefficients and estimating phycocyanin concentration. *Remote Sensing of Environment*, in review.

Li, L., Li, L., Shi, K., Li, Z., & Song, K. An analytical algorithm for remote estimation of phycocyanin in inland waters. *Remote Sensing of Environment*, in preparation.